

An experimental study of the surface thermal signature of hot subaerial isoviscous gravity currents: Implications for thermal monitoring of lava flows and domes

F. Garel,¹ E. Kaminski,¹ S. Tait,¹ and A. Limare¹

Received 22 July 2011; revised 23 November 2011; accepted 23 November 2011; published 7 February 2012.

[1] Management of eruptions requires a knowledge of lava effusion rates, for which a safe thermal proxy is often used. However, this thermal proxy does not take into account the flow dynamics and is basically time-independent. In order to establish a more robust framework that can link eruption rates and surface thermal signals of lavas measured remotely, we investigate the spreading of a hot, isoviscous, axisymmetric subaerial gravity current injected at constant rate from a point source onto a horizontal substrate. We performed laboratory experiments and found that the surface thermal structure became steady after an initial transient. We develop a theoretical model for a spreading fluid cooled by radiation and convection at its surface that also predicts a steady thermal regime. We show that, despite the model's simplicity relative to lava flows, it yields the correct order of magnitude for the effusion rate required to produce the radiant flux measured on natural lava flows. For typical thermal lava properties and an effusion rate between 0.1 and 10 m³ s⁻¹, the model predicts a steady radiated heat flux ranging from 10⁸ to 10¹⁰ W. The assessed effusion rate varies quasi-linearly with the steady heat flux, with much weaker dependence on the flow viscosity. This relationship is valid only after a transient time which scales as the diffusive time, ranging from a few days for small basaltic flows to several years for lava domes. The thermal proxy appears thus less reliable to follow sharp variations of the effusion rate during an eruption.

Citation: Garel, F., E. Kaminski, S. Tait, and A. Limare (2012), An experimental study of the surface thermal signature of hot subaerial isoviscous gravity currents: Implications for thermal monitoring of lava flows and domes, *J. Geophys. Res.*, 117, B02205, doi:10.1029/2011JB008698.

1. Introduction

[2] The eruption rate is the key parameter controlling the impact of volcanic eruptions, and its assessment is crucial for the monitoring of an eruptive crisis. This is true in effusive eruptions, where effusion rate has for example been shown to control strongly the final length a lava flow might attain [e.g., Walker, 1973], as in explosive eruptions where eruption rate controls the height of the plume as well as the ash injection rate [Kaminski *et al.*, 2011]. The estimate of the effusion rate, through measurements of volume increments with time, or by using gas or geophysical proxies, remains both uncertain and hard to achieve in near real time [Harris *et al.*, 2007b]. The use of infrared remote sensing as a near real time monitoring tool has been growing, with the development of the MODVOLC alert system [Wright *et al.*, 2004] and of a thermal proxy for the lava flow effusion rate [e.g., Harris *et al.*, 2007b].

[3] The thermal proxy is based on the work of *Pieri and Baloga* [1986], in which the lava flow is modeled as an unconfined, two-dimensional flow with a constant flow rate, a constant horizontal velocity, a stationary shape (height and width), and a constant surface temperature. Based on these assumptions, *Pieri and Baloga* [1986] derived a relationship relating the effusion rate and the area of the flow when it has fully stopped. From this work, Harris and coworkers [e.g., Harris *et al.*, 1997a; Wright *et al.*, 2001; Harris *et al.*, 2007b] proposed a relationship between the effusion rate and instantaneous heat loss over the lava "active" area, assuming a time-averaged thermal budget of the lava flow. Such use of the formalism of *Pieri and Baloga* [1986] remains a subject of debate [Dragoni and Tallarico, 2009; Harris and Baloga, 2009], nonetheless it is now routinely used in effusive eruptions. Part of the debate arises from the rather crude physical description of the flow used in this formalism, that does not account for a coupling between spreading and cooling. The motivation of this study was to establish a firmer physical basis for interpreting thermal data from lava flows, and, for example, to test the validity of a time-independent relationship between the flow rate and the surface thermal signal using a more consistent fluid dynamic approach.

[4] We model the spreading of lava flows as gravity currents, i.e., currents spreading under their own weight. This

¹Équipe de Dynamique des Fluides Géologiques, Institut de Physique du Globe de Paris, Sorbonne Paris Cité, Université Paris Diderot, UMR CNRS 7154, Paris, France.

Table 1. Experimental Parameters and Conditions^a

| Experiment | \dot{Q} (m ³ s ⁻¹) | Duration | T_0 (°C) | T_a (°C) | μ_0^b (Pa s) | ρ_0^b (kg m ⁻³) |
|------------|--|------------|---------------|---------------|---------------------|-------------------------------------|
| M4 | 7.0 10 ⁻⁷ | 6 min | T_a | 20 | 5.2 | 974 |
| M5 | 3.5 10 ⁻⁷ | 14 min | T_a | 20 | 5.2 | 974 |
| M10 | 3.4 10 ⁻⁷ | 15 min | T_a | 19 | 5.3 | 975 |
| M13 | 3.4 10 ⁻⁷ | 15 min | T_a | 20 | 5.2 | 974 |
| M23 | 1.0 10 ⁻⁷ | 25 min | T_a | 21 | 5.1 | 973 |
| F2 | 1.6 10 ⁻⁹ | 8 h 51 min | T_a | 20 | 13.7 | 974 |
| F5 | 2.0 10 ⁻⁹ | 7 h 13 min | T_a | 16 | 15.0 | 978 |
| F6 | 3.1 10 ⁻⁹ | 8 h 25 min | T_a | 16 | 15.0 | 978 |
| M17 | 7.0 10 ⁻⁸ | 57 min | 56 | 20 | 2.7 | 942 |
| M18 | 6.8 10 ⁻⁸ | 57 min | 50 | 22 | 2.9 | 947 |
| M19 | 8.9 10 ⁻⁸ | 49 min | 56 | 20 | 2.7 | 942 |
| M20 | 1.3 10 ⁻⁷ | 32 min | 55 | 20 | 2.7 | 943 |
| C1 | 3.0 10 ⁻⁸ | 1 h 35 min | 52 | 18 | 2.9 | 945 |
| C7 | 4.0 10 ⁻⁸ | 1 h 12 min | 44 | 17 | 3.3 | 952 |
| C14 | 2.2 10 ⁻⁸ | 2 h 15 min | 42 | 20 | 3.4 | 954 |

^aThe emissivity ε , specific heat C_p , thermal conductivity k , and thermal diffusivity κ for 47V 5000 oil are 0.96, 1500 J kg⁻¹ K⁻¹, 0.15 W m⁻¹ K⁻¹, and 10⁻⁷ m² s⁻¹, respectively. The thermal conductivity k_s and diffusivity κ_s of the polystyrene are about 0.03 W m⁻¹ K⁻¹ and 6 × 10⁻⁷ m² s⁻¹.

^bHere μ_0 and ρ_0 are the viscosity and density at source temperature T_0 (ambient temperature for the isothermal experiments). The viscosities of the silicone oils vary by less than a factor of 2 for the working temperature range (20°C–60°C).

framework has been used to model the growth of volcanic domes [Huppert *et al.*, 1982; Sakimoto and Zuber, 1995; Griffiths and Fink, 1997; Balmforth *et al.*, 2004] and the dynamics of lava flows [Fink and Griffiths, 1990; Stasiuk *et al.*, 1993; Blake and Bruno, 2000; Michaut and Bercovici, 2009]. Since the pioneer study of an isothermal Newtonian gravity current by Huppert [1982], various rheologies and geometries have been investigated [Griffiths and Fink, 1992; Bercovici, 1994; Tallarico and Dragoni, 2000; Sakimoto and Gregg, 2001; Griffiths *et al.*, 2003; Lyman *et al.*, 2004; Balmforth *et al.*, 2006; Ancy and Cochard, 2009]. The thermal evolution of viscous gravity currents has been studied numerically by Bercovici [1994], Bercovici and Lin [1996], Balmforth and Craster [2000], and Balmforth *et al.* [2004] and experimentally by Stasiuk *et al.* [1993]. These studies showed that, after a transient stage, a

thermal steady state was reached, but did not explore the surface thermal structure as a function of the supply rate and thermal boundary conditions. Hence, they did not make a direct link between the input rate and the thermal signal that it is now possible to measure regularly.

[5] The present study aims at bridging the gap between theoretical modeling of gravity currents and more empirical interpretation of satellite thermal images of active lava flows. We derive a first-order reference model for lava flows to test the ability of the surface thermal structure to reflect the volumetric magma flux under well-defined and controlled conditions. We consider horizontal, axisymmetric subaerial gravity current with a Newtonian isoviscous rheology, focusing on the thermal evolution of the surface of the flow. We do not try to reproduce the full complexity of thermal and mechanical features observed in natural lava flows, but instead investigate the evolution of the radiant flux as a function of the effusion rate for a simple model to give first-order results of the applicability of a thermal proxy for the effusion rate. We perform laboratory experiments and analyze the data by means of a theoretical model, based on work by Huppert [1982]. The model, once validated by the comparison with the experimental observations, is used to predict the surface signature of lava flows in conditions similar to those of the experiments. We then discuss the implications of our study for natural lava flows, and outline future possible improvements of the model to go beyond its present limitations.

2. Laboratory Experiments

2.1. Experimental Methods

[6] We observe the flow and cooling of silicone oil (Rhodorsil® 47V 5000 or 47V 12500, dyed red), initially at a temperature T_0 , as it spreads horizontally, when injected at a constant supply rate \dot{Q} from a point source, into air (at temperature $T_a \leq T_0$) onto a polystyrene plate. The latter was covered either with plastic or Teflon film. Table 1 gives details of the experimental parameters and conditions. A sketch of the experimental apparatus is presented in Figure 1.

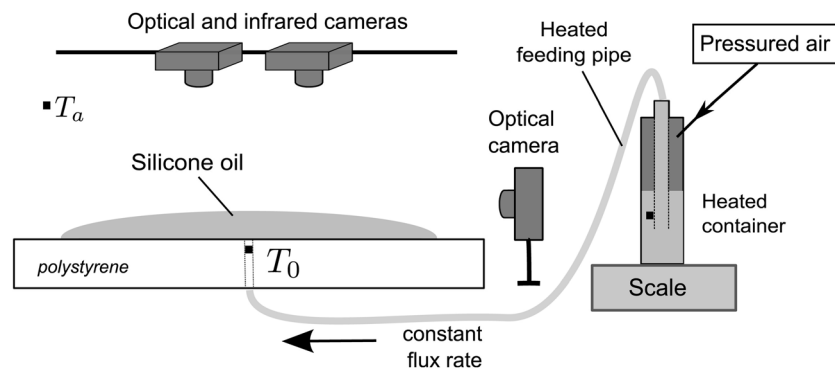


Figure 1. Experimental setup. Oil is supplied through a pipe (2 or 4 mm radius) at a constant rate driven by a constant air overpressure in the source vessel. The injection is made either from below (as in the sketch) or from above. The oil reservoir is kept at constant temperature. A thermocouple (black square) placed at the end of the pipe measures the source temperature T_0 . The radial extent of the current is measured on pictures taken from above, whereas the surface temperatures are measured either with an infrared camera or with a radiometer.

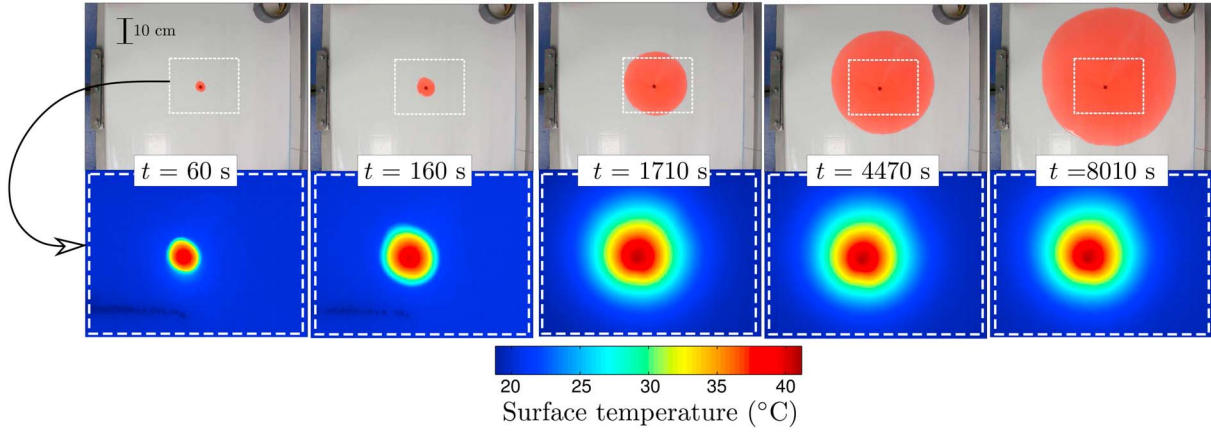


Figure 2. Optical and infrared images taken during experiment C14. The dynamic evolution can be seen in Animation 1. The dashed rectangle in the optical image corresponds to the field of view of the infrared image below.

2.2. Evolution of Surface Thermal Structure

[7] The evolution of the surface temperature of the current T_{top} is shown in Figure 2 and Animation 1 for a reference experiment (C14).¹ The spreading oil and its surface thermal structure both display quasi-axisymmetric geometry, but after some time, the thermal structure reaches a steady state although the oil continues to spread. We characterize the size of the thermal anomaly through a threshold “thermal” radius $r_c(t)$ such that (Figure 3a)

$$T_{top}(r=0, t) - T_{top}(r_c, t) = \frac{95}{100} [T_{top}(r=0, t) - T_a]. \quad (1)$$

The size of the anomaly $r_c(t)$ first increases with $R_N(t)$ the radial extent of the viscous current, until it reaches a constant value R_c (Figure 3b). R_c provides a thermal time scale t_c through the scaling of the viscous spreading, taking $R_N(t_c) = R_c$.

[8] A thermal steady state is reached in all our “hot” experiments (Table 2). This was predicted both by *Bercovici and Lin* [1996] for a viscous flow with a highly temperature-dependent viscosity, and by *Balmforth and Craster* [2000] and *Balmforth et al.* [2004] for a viscoplastic fluid. It was also suggested from experimental observations made by *Stasiuk et al.* [1993] on glucose syrup injected beneath cold water. Here we characterize the intensity and the spatial extent of the thermal anomaly at steady state through its thermal radius R_c , and its radiated heat flux $\overline{\phi_{rad}}$ defined as the steady value of

$$\overline{\phi_{rad}}(t) = 2\pi \int_0^{R_N(t)} r \varepsilon \sigma (T_{top}^4(r, t) - T_a^4) dr, \quad (2)$$

with σ the Stefan-Boltzmann constant (Figure 4).

[9] In section 3, we develop a simple theoretical model to characterize $\overline{\phi_{rad}}$ and R_c as a function of the parameters of the current and the cooling boundary conditions.

3. Theoretical Model

3.1. Governing Equations

[10] We model the horizontal axisymmetric spreading of an isoviscous fluid of density ρ and viscosity μ , supplied at

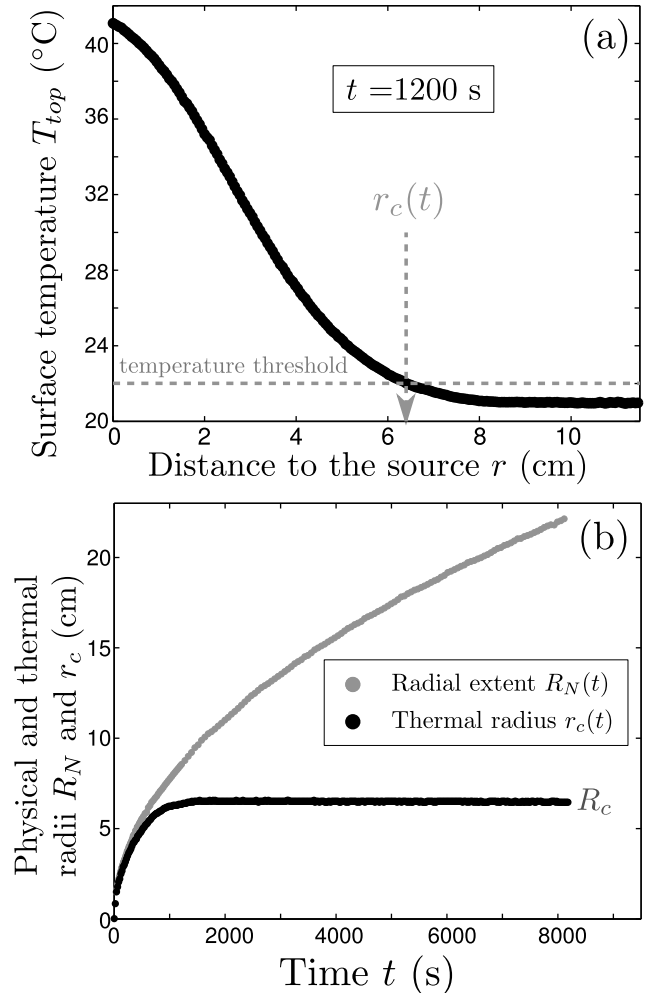


Figure 3. (a) Steady radial surface temperature profile during experiment C14. The temperature threshold (equation (1)) defines the thermal radius r_c . (b) Evolution of thermal radius $r_c(t)$ and of physical extent of the current $R_N(t)$ during experiment C14. The radial extent of the current $R_N(t)$ continuously increases as the square root of time, whereas $r_c(t)$ reaches a plateau value R_c after ≈ 1000 s.

¹Animation 1 is available in the HTML.

Table 2. Experimental Surface Thermal Steady State

| Experiment | $\overline{\phi_{rad}}$ (W) | R_c (cm) | t_c (s) |
|------------|--------------------------------|---------------|--------------|
| M17 | 2.5–3.2 | 11.2–12.9 | 1200–1570 |
| M18 | 1.7–2.2 | 10.6–11.9 | 1070–1330 |
| M19 | 3.0–3.5 | 11.7–13.2 | 1075–1350 |
| M20 | 4.6–5.0 | 13.4–15.3 | 970–1250 |
| C1 | 0.86–0.94 | 7.2–7.8 | 700–830 |
| C7 | 0.81–1.00 | 8.1–8.8 | 640–780 |
| C14 | 0.45–0.49 | 6.5–6.7 | 675–735 |

temperature T_0 and constant volumetric rate Q , into a medium of density $\rho_a \ll \rho$, viscosity μ_a ($\mu \gg \mu_a \approx 0$), and temperature $T_a \leq T_0$ (Figure 5 and Table 3). For this flow, Huppert [1982] derived local mass and momentum conservations at low Reynolds number in cylindrical coordinates, under the lubrication approximation, i.e., such that the extent of the current is much greater than its height. In the same approximation, and neglecting viscous dissipation as a heat source, the local energy conservation equation is written as

$$\frac{\partial T}{\partial t} + u \frac{\partial T}{\partial r} + w \frac{\partial T}{\partial z} = \kappa \frac{\partial^2 T}{\partial z^2}, \quad (3)$$

where $T(r, z, t)$ is the current temperature, $w(r, z, t)$ and $u(r, z, t)$ are the vertical (along z) and horizontal (along r) current velocities, respectively, $\kappa = \frac{k}{\rho C_p}$ is the thermal diffusivity, with k the thermal conductivity, and C_p the specific heat of the fluid.

[11] We transform the local energy equation (3) into a global energy budget by integration over z , using the continuity equation and assuming a kinematic condition at the surface of the flow:

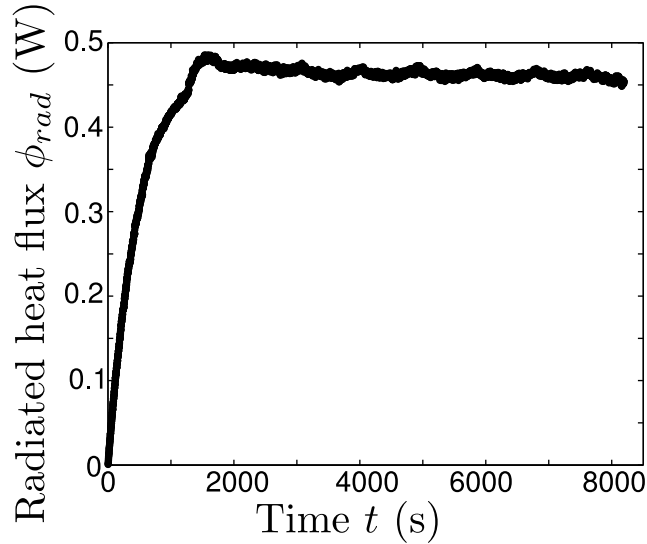


Figure 4. Heat flux radiated by the current, ϕ_{rad} , as a function of time for experiment C14. The oscillations in the steady state are due to the temperature variations during air-conditioning cycles.

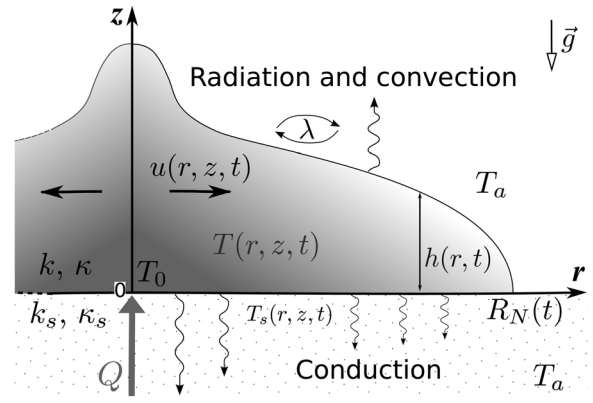


Figure 5. Schematic representation of the spreading isoviscous gravity current. Physical parameters and variables are listed in Table 3.

$$\frac{\partial}{\partial t} \left(\int_0^{h(r,t)} T dz \right) = -\frac{1}{r} \frac{\partial}{\partial r} \left(r \int_0^{h(r,t)} u T dz \right) + \kappa \left(\frac{\partial T}{\partial z} \Big|_{z=h} - \frac{\partial T}{\partial z} \Big|_{z=0} \right), \quad (4)$$

where $h(r, t)$ is the current thickness. Using the expression of flow velocity $u(r, z, t)$ [Huppert, 1982], the energy budget (4) becomes

$$\frac{\partial}{\partial t} \left(\int_0^{h(r,t)} T dz \right) = \frac{\Delta \rho g}{2\mu} \frac{1}{r} \frac{\partial}{\partial r} \left(r \frac{\partial h}{\partial r} \int_0^{h(r,t)} z(2h-z) T dz \right) + \kappa \left(\frac{\partial T}{\partial z} \Big|_{z=h} - \frac{\partial T}{\partial z} \Big|_{z=0} \right), \quad (5)$$

Table 3. Model Parameters

| Symbol | Description | Units |
|-------------------------|--|----------------------------------|
| Q | constant volumetric supply rate | $\text{m}^3 \text{s}^{-1}$ |
| T_0 | source temperature | K |
| ρ | fluid density | kg m^{-3} |
| ρ_a | ambient density | kg m^{-3} |
| μ | fluid viscosity | Pa s |
| ε | fluid emissivity | - |
| k | fluid thermal conductivity | $\text{W m}^{-1} \text{K}^{-1}$ |
| C_p | fluid specific heat | $\text{J kg}^{-1} \text{K}^{-1}$ |
| κ | fluid thermal diffusivity | $\text{m}^2 \text{s}^{-1}$ |
| T_a | ambient and initial substrate temperature | K |
| λ | convective heat transfer coefficient | $\text{W m}^{-2} \text{K}^{-1}$ |
| k_s | thermal conductivity of the substrate | $\text{W m}^{-1} \text{K}^{-1}$ |
| κ_s | thermal diffusivity of the substrate | $\text{m}^2 \text{s}^{-1}$ |
| $T_{top}(r, t)$ | surface temperature of the current | K |
| $T_{base}(r, t)$ | base temperature of the current | K |
| $\overline{T}(r, t)$ | vertically averaged temperature of the current | K |
| $T_s(r, z, t)$ | temperature of the substrate | K |
| $h(r, t)$ | height of the current | m |
| $u(r, z, t)$ | horizontal velocity of the current | m s^{-1} |
| $w(r, z, t)$ | vertical velocity of the current | m s^{-1} |
| $R_N(t)$ | radial extent of the current | m |
| τ | characteristic diffusive time scale | s |
| $r_c(t)$ | thermal radius | m |
| $\phi_{rad}(t)$ | radiative heat flux from the current | W |
| R_c | steady state thermal radius | m |
| $\overline{\phi_{rad}}$ | steady state radiated heat flux | W |
| t_c | cooling time scale | s |

where $\Delta\rho = \rho - \rho_a$ is the density difference between the fluid and the environment and g is the acceleration of gravity. *Balmforth et al.* [2004] demonstrated that the integral formulation equation (4) leads to results similar with the full numerical solution of the heat equation [*Balmforth et al.*, 2004, Figure 8].

[12] This budget equation introduces two explicit boundary conditions. At the upper surface, heat is lost by radiation and convection:

$$-k \frac{\partial T}{\partial z} \Big|_{z=h(r,t)} = \varepsilon\sigma [T_{top}(r,t)^4 - T_a^4] + \lambda [T_{top}(r,t) - T_a], \quad (6)$$

where λ is the convective heat transfer coefficient characterizing the strength of convection in the air, according to the empirical ‘‘Newton’s law’’. This represents a linear approximation for free convection, that has only small impact on the calculated temperature solution. At the base of the current, heat is lost by conduction:

$$k \frac{\partial T}{\partial z} \Big|_{z=0^+} = k_s \frac{\partial T_s}{\partial z_s} \Big|_{z_s=0^-} \quad (7)$$

with T_s the temperature in the substrate.

3.2. Dimensionless Equations

[13] The dimensions of the current are given by its radial extent $R_N(t)$ and a reference height h_{ref} derived by *Huppert* [1982]:

$$R_N(t) = a \left(\frac{\Delta\rho g Q^3}{3\mu} \right)^{\frac{1}{8}} t^{\frac{1}{2}} \quad (8)$$

$$h_{ref} = a^{\frac{2}{5}} \left(\frac{3\mu Q}{\Delta\rho g} \right)^{\frac{1}{4}}, \quad (9)$$

where $a \simeq 0.715$ is a dimensionless constant [*Huppert*, 1982], derived from a global mass conservation equation. The thermal evolution of the flow is characterized by the source temperature T_0 and the diffusive time scale for vertical heat conduction $\tau = \frac{h_{ref}^2}{\kappa}$. This scaling is used to introduce the following dimensionless variables:

$$\begin{aligned} T^*(r^*, z^*, t^*) &= \frac{T}{T_0}, \\ T_s^*(r^*, z_s^*, t^*) &= \frac{T_s}{T_0}, \\ t^* &= \frac{t}{\tau}, \\ r^* &= \frac{r}{R_N(t)}, \\ \psi(r^*) &= \frac{h(r,t)}{h_{ref}}, \\ z^* &= \frac{z}{h(r,t)} = \frac{z}{\psi(r^*)\sqrt{\kappa\tau}}, \\ z_s^* &= \frac{z_s}{\sqrt{\kappa_s\tau}}, \end{aligned}$$

yielding the dimensionless energy conservation equation

$$\begin{aligned} \psi \frac{\partial}{\partial t^*} \left(\int_0^1 T^* dz^* \right) - \frac{r^*}{2t^*} \frac{\partial}{\partial r^*} \left(\psi \int_0^1 T^* dz^* \right) - \frac{3}{2} \frac{1}{t^*} \frac{1}{r^*} \frac{\partial}{\partial r^*} \\ \cdot \left(r^* \psi^3 \frac{d\psi}{dr^*} \int_0^1 z^* (2-z^*) T^* dz^* \right) = \frac{1}{\psi} \left(\frac{\partial T^*}{\partial z^*} \Big|_{z^*=1} - \frac{\partial T^*}{\partial z^*} \Big|_{z^*=0} \right), \end{aligned} \quad (10)$$

where ψ is the shape function of the current defined by *Huppert* [1982].

[14] The surface and basal cooling conditions (6) and (7) become

$$\begin{aligned} -\frac{1}{\psi} \frac{\partial T^*}{\partial z^*} \Big|_{z^*=1} = N_{surf} \left\{ (1-N_\lambda) [T_{top}^{*4} - (1-N_T)^4] \right. \\ \left. + N_\lambda [T_{top}^* - (1-N_T)] \right\} \end{aligned} \quad (11)$$

$$\frac{1}{\psi} \frac{\partial T^*}{\partial z^*} \Big|_{z^*=0^+} = N_{base} \frac{\partial T_s^*}{\partial z_s^*} \Big|_{z_s^*=0^-}. \quad (12)$$

The thermal boundary conditions give rise to dimensionless numbers, defined as follows:

$$\begin{cases} N_T = \text{Relative energy content} = \frac{T_0 - T_a}{T_0} \\ N_{surf} = \frac{\text{Total heat flux at the surface}}{\text{Vertical heat diffusion in the current}} = \frac{\varepsilon\sigma T_0^4 + \lambda T_0}{k \frac{T_0}{h_{ref}}} \\ N_\lambda = \frac{\text{Convective heat flux at the surface}}{\text{Total heat flux at the surface}} = \frac{\lambda}{\varepsilon\sigma T_0^3 + \lambda} \\ N_{base} = \frac{\text{Conductive heat flux at the base of the current}}{\text{Vertical heat diffusion in the current}} \\ = \frac{k_s}{k} \sqrt{\frac{\kappa}{\kappa_s}}. \end{cases} \quad (13)$$

3.3. Numerical Resolution

[15] To obtain an approximate temperature solution of equation (10), we use an integral method based on a second-order polynomial expression of the temperature, following *Bercovici and Lin* [1996], which directly satisfies the boundary conditions

$$\begin{aligned} T^*(r^*, z^*, t^*) &= 6\bar{T}^*(r^*, t^*) \times (z^* - z^{*2}) + T_{top}^*(r^*, t^*) \\ &\quad \times (3z^{*2} - 2z^*) + T_{base}^*(r^*, t^*) \times (3z^{*2} - 4z^* + 1), \end{aligned} \quad (14)$$

where $\bar{T}^*(r^*, t^*) = \int_0^1 T^* dz^*$. This is combined with a numerical solution for the dimensionless height ψ [see *Huppert*, 1982]. Since we are explicitly interested in the surface temperature, we do not model a vertically isothermal current. Equations (10) and (11) are solved with an implicit numerical method, with equation (12) having an explicit solution. The boundary conditions for temperature are $T^*(r^* = 0, z^* = 0, t^*) = 1$ and $T^*(r^* = 1, z^*, t^*) = 1 - N_T$.

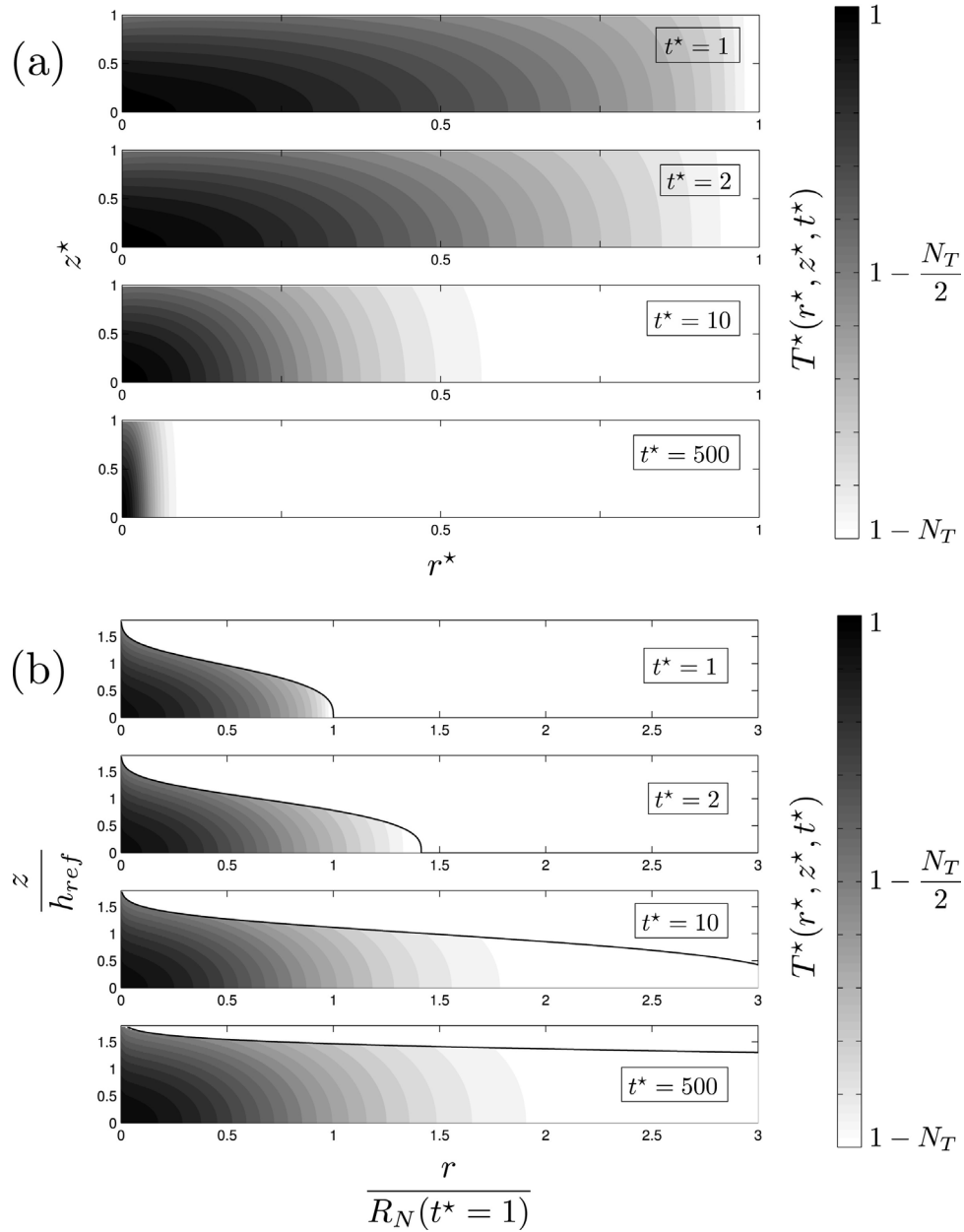


Figure 6. Time evolution of temperature structure in the current for $N_T = 0.5$, $N_\lambda = 0.5$, $N_{surf} = 1$, and $N_{base} = 0$. (a) Temperature structure in the dimensionless frame defined by the spreading of the current. (b) Temperature structure and advance of the current in an alternative dimensionless frame. The solid line is the shape of the current.

[16] The vertical temperature profile in the substrate, T_s , is [Carlsaw and Jaeger, 1959, p. 63]

$$T_s(r, z_s, t) - T_a = \frac{-z_s}{2\sqrt{\pi\kappa_s}} \int_0^t \frac{T_{base}(r, \zeta) - T_a}{(t - \zeta)^{3/2}} e^{-\frac{z_s^2}{4\kappa_s(t-\zeta)}} d\zeta, \quad (15)$$

where $T_{base} = T(r, z = 0, t)$ is the temperature at the base of the current, which can be approximated to first order by Carlsaw and Jaeger [1959, p. 63]

$$T_s(r, z_s, t) - T_a = (T_{base}(r, t) - T_a) \operatorname{erfc} \frac{-z_s}{2\sqrt{\kappa_s t}}, \quad (16)$$

leading to the dimensionless basal heat flux

$$\frac{1}{\psi} \frac{\partial T^*}{\partial z^*} \Big|_{z^*=0^+} = N_{base} \frac{T_{base}^* - (1 - N_T)}{\sqrt{\pi t^*}}. \quad (17)$$

4. Results

4.1. Reference Numerical Solution: Two-Stage Cooling

[17] Before exploring the full range of solutions, we first present a reference solution for “average” values of the

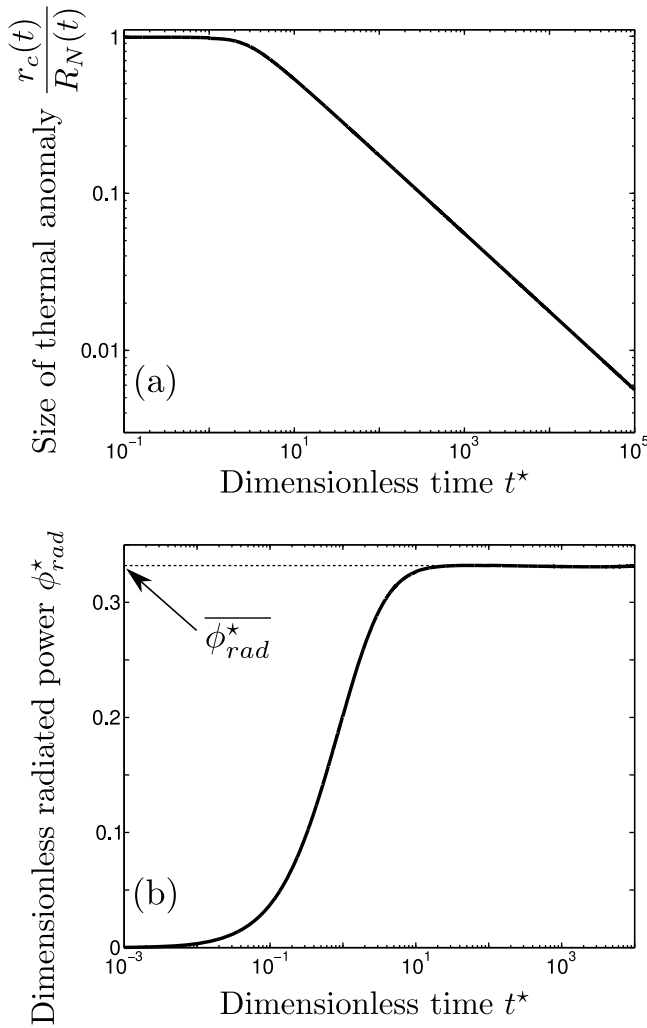


Figure 7. Time evolution of (a) the size r_c of the thermal anomaly relative to the extent of the current $R_N(t)$ and (b) dimensionless radiant heat flux ϕ_{rad}^* for $N_T = 0.5$, $N_\lambda = 0.5$, $N_{surf} = 1$, and $N_{base} = 0$. The evolution of $r_c(t)/R_N(t)$ for $t^* > 10$ approximately follows $\approx t^{-0.5}$, which corresponds to a surface thermal quasi steady state ($r_c(t) = R_c$).

following dimensionless numbers: $N_T = 0.5$, $N_\lambda = 0.5$ and $N_{surf} = 1$. N_{base} is furthermore set to 0 which corresponds to an adiabatic substrate.

[18] The thermal structure of the current is presented in Figure 6. In the dimensionless frame of Figure 6a, the temperature structure reflects the spreading of the current and the relative shrinking of the thermal anomaly, that becomes confined to the neighborhood of the source. The radial temperature structure of the thermal anomaly (Figure 6b) can be interpreted in a Lagrangian framework as the progressive cooling of a column of hot fluid as it moves away from the source. The surface temperature structure appears constant for $t^* > 10$. At a given location the flow thickness increases with time, hence the current continues to store thermal energy though the surface temperature remains constant.

[19] Figure 7 presents the two-stage evolution (1) of the size of the thermal anomaly r_c , defined as in equation (1),

relative to the radial extent of the current, and (2) of the dimensionless radiated heat flux ϕ_{rad}^* defined as

$$\phi_{rad}^*(t^*) = [\rho C_p Q (T_0 - T_a)]^{-1} \phi_{rad}(t) \quad (18)$$

$$\phi_{rad}^*(t^*) = 2\pi a^3 N_{surf} t^* \int_0^1 r^* (1 - N_\lambda) \frac{T_{top}^{*4}(r^*, t^*) - (1 - N_T)^4}{N_T} dr^* \quad (19)$$

In the first stage, the relative size of the thermal anomaly is almost constant (i.e., $r_c(t)$ follows the rate of spreading) while the dimensionless radiant flux increases. In the second stage, ϕ_{rad}^* reaches a plateau value $\overline{\phi_{rad}^*}$ and the relative size of the thermal anomaly decreases approximately as $t^{-0.5}$. This corresponds to first order as the sole evolution of $R_N(t)$ (equation (8)), hence to a quasi-steady surface temperature structure, with $r_c(t) = R_c$, as in the experiments. For two-phase gravity currents such as degassing lava flows, *Michaut and Bercovici* [2009] also predicted a steady fluid fraction near the constant rate injection point. They define a “loss radius” where all the fluid phase has been degassed, somewhat analogous to that observed here for the temperature field.

4.2. Cross-Validation of Experimental and Theoretical Results

[20] Experiments, unlike real volcanic eruptions, are performed in controlled conditions: the theoretical predictions for a set, constant input rate can be compared to the experimental observations, to validate both the physics and the numerical method used to solve the theoretical problem.

[21] The comparison between experimental and theoretical spreadings is very good (see Appendix A) and confirms the results of *Huppert* [1982]. Figure 8 presents experimental and predicted surface temperature profiles for experiment C14. The value of N_λ corresponds to an average value of $\lambda = 2 \pm 1 \text{ W m}^{-2} \text{ K}^{-1}$ for free convection. The experimental data are obtained through an average of ten profiles across the oil pancake. At $t^* = 5$, we observe some discrepancy between the experimental data and the theoretical model. We interpret the faster experimental cooling as due to lateral heat conduction in the substrate that initially widens the size of the thermal anomaly. This effect decreases as the temperature decreases at the front of the current, and becomes negligible for $t^* > 10$, when the experimental observations are well reproduced by theory.

[22] The comparison between experimental and theoretical values of the parameters that characterize the steady state thermal structure ($\overline{\phi_{rad}^*}$ and R_c) is shown in Figure 9 for all the experiments. All the data align well with the theoretical predictions, which shows that the model is physically consistent, and which provides us with a firm basis to further study the thermal structure of a gravity current as a function of the dimensionless numbers defined in section 3.2.

4.3. Complete Solutions

[23] We first investigate the thermal features of the surface steady state as a function of the dimensionless numbers N_T , N_λ and N_{surf} . N_{base} influences only the transient thermal evolution of the current, and is considered later.

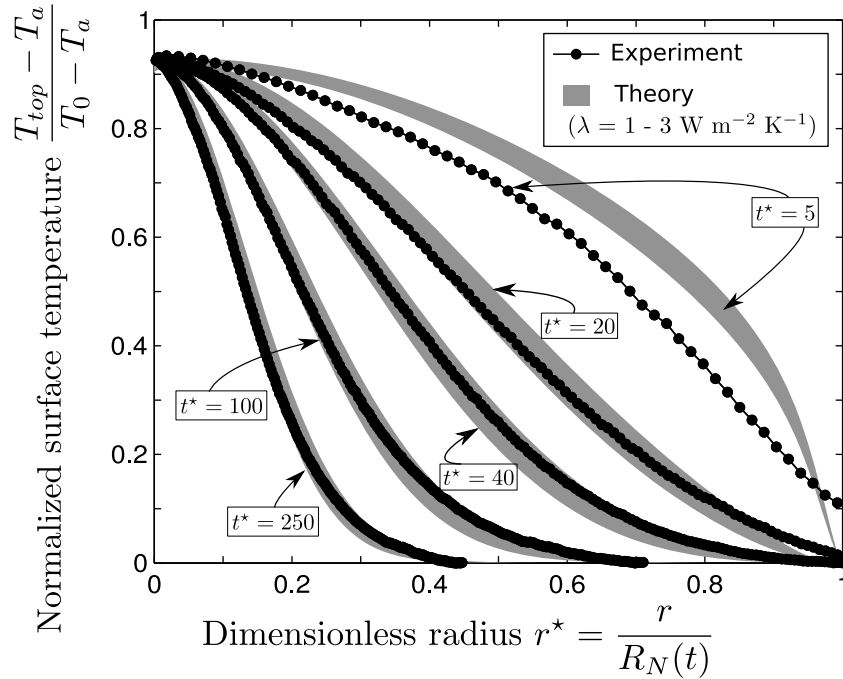


Figure 8. Comparison of experimental and model normalized surface temperatures during experiment C14 for $N_T = 0.07$, $N_{base} = 0.08$, and either $N_\lambda = 0.36$ and $N_{surf} = 0.033$ ($\lambda = 1 \text{ W m}^{-2} \text{ K}^{-1}$) or $N_\lambda = 0.63$ and $N_{surf} = 0.057$ ($\lambda = 3 \text{ W m}^{-2} \text{ K}^{-1}$). The initial discrepancy is due to lateral heat conduction in the substrate. For times larger than $t^* \approx 10$, the model accounts well for the observations.

4.3.1. Surface Thermal Signature of the Current at Steady State

[24] The thermal surface steady state described in section 4.1 reflects a global balance between heat lost at the surface of the current and heat advected within the flow, hence should depend mainly on N_{surf} . This can be illustrated by rewriting N_{surf} as

$$N_{surf} = \frac{(\varepsilon\sigma T_0^4 + \lambda T_0)R_N(\tau)^2}{\rho C_p Q T_0 U_{ref} h_{ref} R_N(\tau)}, \quad (20)$$

where we have introduced U_{ref} , a characteristic velocity for horizontal heat advection in the lubrication theory, derived from Huppert [1982]:

$$U_{ref} = \frac{\rho g}{3\mu} \frac{h_{ref}^3}{R_N(\tau)}. \quad (21)$$

[25] The influence of N_{surf} , the ratio of surface heat flux and vertical heat diffusion, on the temperature structure of the current, is shown in Figure 10. For small N_{surf} heat loss at the surface is very small, and efficient heat conduction results in a vertically isothermal current. We may expect this kind of internal thermal structure in our experiments. In the limit of large N_{surf} , the poor vertical heat transfer yields a strong vertical temperature gradient, leading to much lower surface temperatures. The temperature field of the current near the source catches the first-order thermal structure of a natural lava flow, but the isoviscous model cannot represent the

temperature jump between the solid crust and the hot interior of a lava flow.

[26] The variations of the dimensionless plateau radiated heat flux $\overline{\phi_{rad}^*}$ are shown in Figure 11. The general shape of $\overline{\phi_{rad}^*}$ as a function of N_{surf} allows one to define two cooling regimes with quite a sharp transition at $N_{surf} = 1$ whatever the value of N_T and N_λ . At small N_{surf} the thermal structure is controlled by internal heat transfer which counterbalances the heat loss at surface. Hence the surface thermal anomaly is larger in this regime and so is the radiated heat flux. At large N_{surf} the surface cooling is the dominant process, yielding a weaker surface thermal anomaly, hence a lower radiated heat flux.

[27] The relative values of $\overline{\phi_{rad}^*}$ in each regime depend additionally on the two other dimensionless numbers N_T and N_λ as shown in Figure 11. This can be simply interpreted as the relative importance of radiation (\mathcal{R}) and convection (\mathcal{C}) at the flow surface (equation (11)):

$$\frac{\mathcal{R}}{\mathcal{C}} \approx \frac{1 - N_\lambda}{N_\lambda} \frac{T_{top}^{*4} - (1 - N_T)^4}{T_{top}^* - (1 - N_T)}, \quad (22)$$

which scales as $\frac{1 - N_\lambda}{N_\lambda} (1 - N_T)^3$. All things being equal, $\overline{\phi_{rad}^*}$ decreases as N_λ (hence convection) increases. The same conclusion holds for increasing N_T though it corresponds to a current with a larger internal heat content.

4.3.2. Size of the Thermal Anomaly at Steady State

[28] The time required to cool down the current cannot be smaller than the diffusive time scale τ , hence R_c has a lower bound value $R_N(\tau)$ (and $t_c \geq \tau$). This extreme regime is

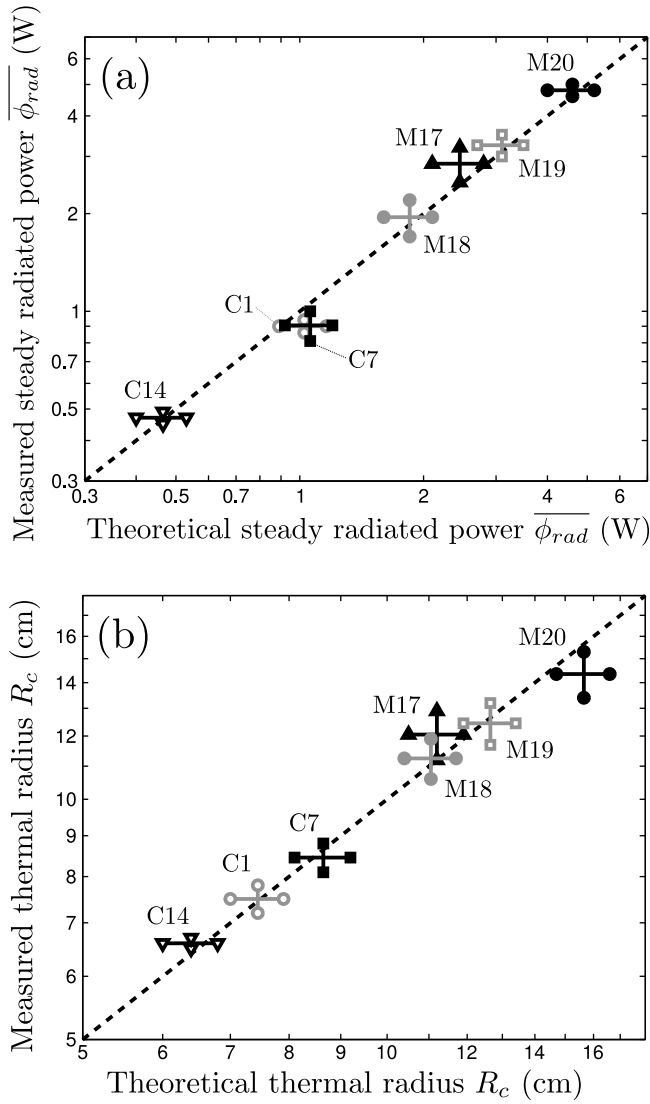


Figure 9. Comparison of experimental and predicted (a) steady radiated heat flux $\overline{\phi_{rad}}$ and (b) steady thermal radius R_c . The theoretical error bar is due to the uncertainty on the convective heat transfer coefficient λ , taken between 1 and 3 W m⁻² K⁻¹, which has an influence on the global surface temperature structure.

expected to occur for a very efficient surface cooling (high N_{surf}). To study the variation of the extent of the surface thermal anomaly as a function of the dimensionless numbers, we introduce a dimensionless thermal radius at steady state, $R_c^* \equiv R_c/R_N(\tau)$.

[29] Figure 12 confirms that, for $N_{surf} \gg 1$, vertical diffusive heat transfer in the current is the limiting process of cooling and $R_c^* \rightarrow 1$. For $N_{surf} \ll 1$, the limiting process is the efficiency of surface cooling, that scales as $N_{surf} R_c^{*2}$. Hence, for a given injected power, the radius of the area required to achieve thermal balance scales as $N_{surf}^{-1/2}$. For any N_{surf} or N_λ , R_c^* increases with the relative energy content N_T because a hotter fluid emitted at the source will take longer to cool down.

4.3.3. Transient Conductive Heat Loss

[30] The efficiency of cooling of the current depends on the temperature of air and of the temperature of the substrate (equations (6) and (7)). Whereas the temperature of ambient air can be taken as constant, the temperature of the substrate increases by heat transfer from the hot current. Consequently, for a given N_{base} , the basal heat flux decreases with time (equation (17)) and eventually becomes null, leading to the same steady thermal structure as in the adiabatic case (Figures 13 and 14a). Hence only the duration of the transient stage is expected to depend on N_{base} .

[31] We define the duration of the transient thermal state as the time required to reach 90% of the plateau radiated heat flux, i.e., $\phi_{rad}^*(t_{90\%}^*) = 0.90\overline{\phi_{rad}^*}$. In the adiabatic case, $t_{90\%}^* \approx t_c^*$. Figure 14 shows the evolution of the dimensionless duration $t_{90\%}^*$ as a function of N_{base} . A more conductive substrate (high N_{base}) delays the establishment of a steady state, and $t_{90\%}^*$ scales to first order with N_{base}^2 in agreement with equation (17).

[32] As a conclusion, our theoretical model, governed by four dimensionless numbers that encompass the role of surface and basal boundary conditions, can reproduce the surface temperature structure observed in the laboratory experiments. The thermal surface signature reaches a steady state after a transient time controlled by the balance between internal diffusion and efficiency of surface cooling. The radiated heat flux at steady state $\overline{\phi_{rad}}$ scales as the product of the supply rate Q and temperature difference $T_0 - T_a$. The size of the thermal anomaly R_c and the duration t_c of the transient stage have lower bounds $R_N(\tau)$ and τ , respectively, set by the limiting diffusion in the cooling process. We now investigate the implication of the model for natural subaerial gravity currents.

5. Discussion

5.1. General Implications of the Isoviscous Cooling Model

[33] We have presented a consistent theoretical model validated by laboratory experiments, where the physical processes involved are clearly identified. However, there are many differences between an isoviscous fluid spreading axisymmetrically on a horizontal plane, and the flow of lava, related to topography and flow rheology, for example. An important issue is thus to discriminate and hierarchize the different parameters likely to play a role in the relationship between the effusion rate and the surface radiant heat flux in more complex natural flows. We start here to build this hierarchy based on the agreement and discrepancies between the model predictions and observations on natural lava flows.

[34] We focus on the radiant heat flux as an integrated thermal signal and possible proxy for the effusion rate of lava flows, if the energy input balances the cooling at the flow surfaces. Figure 15 presents the relative influence of the flow parameters on the thermal evolution of an ideal lava flow. The steady state heat flux radiated by the current is much more dependent on the effusion rate Q than on the viscosity μ , and quasi-proportional to Q . Hence, if the petrological characteristics of the lava are not well known, a robust estimate of the effusion rate is still possible, but only assuming that the steady state regime has been reached. For terrestrial

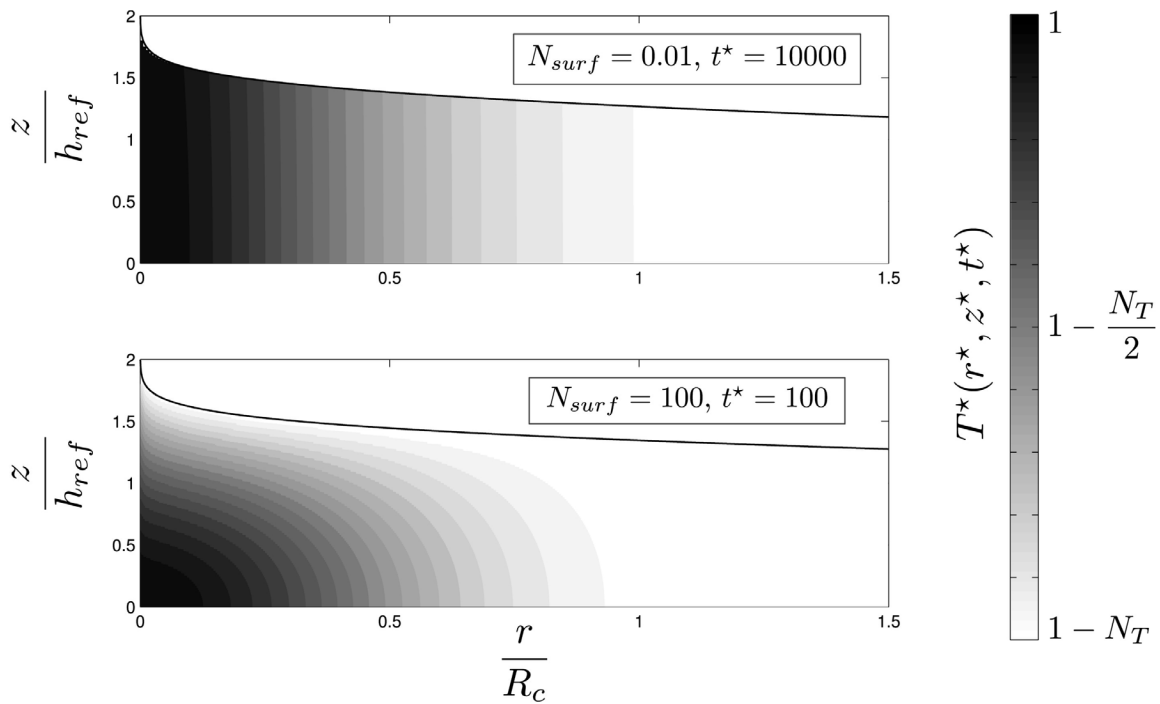


Figure 10. Temperature structure in the current for $N_T = 0.5$, $N_\lambda = 0.5$, $N_{base} = 0$, and either (top) $N_{surf} = 0.01$ ($t^* = 10000$) or (bottom) $N_{surf} = 100$ ($t^* = 100$). The surface thermal steady state has been reached in both cases, and the part of the current located at $r > R_c$ is almost at ambient temperature. The dimensionless thermal radii (R_c^*) are about 16 and 1 for $N_{surf} = 0.01$ and $N_{surf} = 100$, respectively.

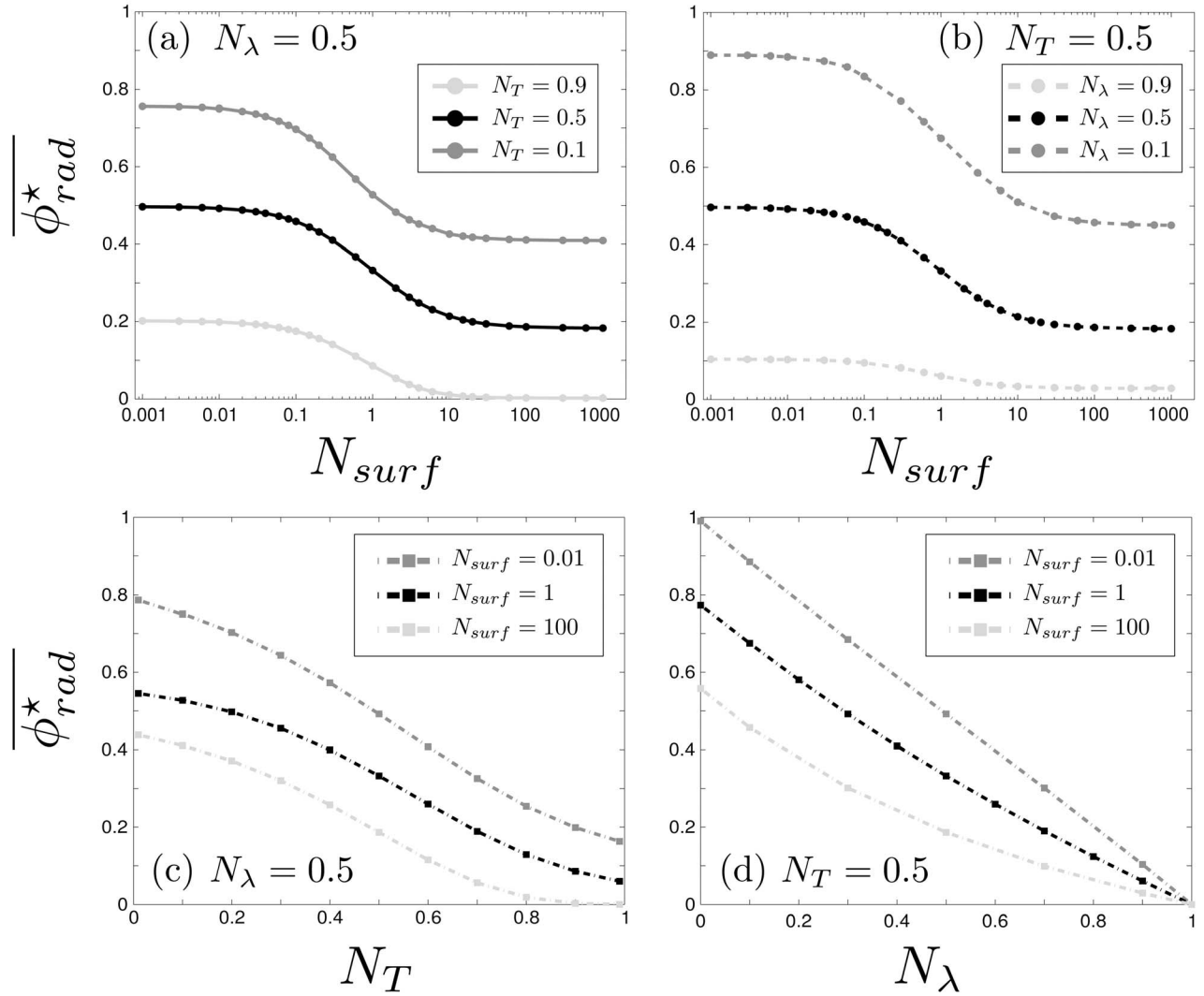


Figure 11. Steady dimensionless radiated power $\overline{\phi_{rad}^*}$ as a function of N_{surf} for $N_{base} = 0$ and either (a) $N_\lambda = 0.5$ and different N_T or (b) $N_T = 0.5$ and different N_λ . Steady dimensionless radiated power $\overline{\phi_{rad}^*}$ (c) as a function of N_T for $N_\lambda = 0.5$ and (d) as a function of N_λ for $N_T = 0.5$ for $N_{surf} = 0.01, 1, \text{ and } 100$.

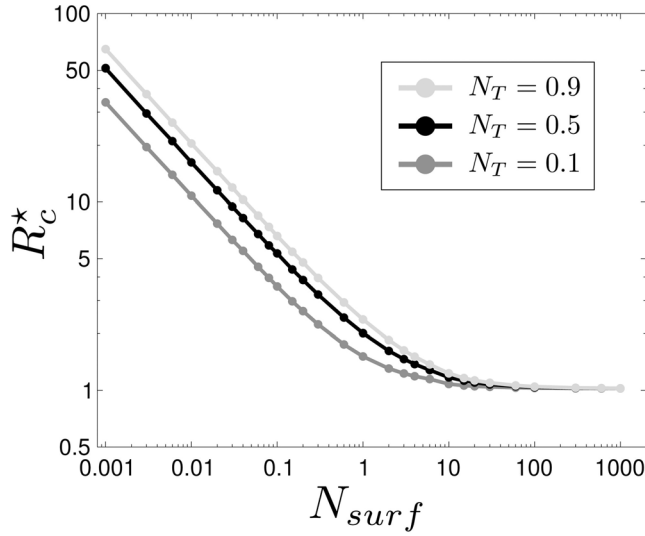


Figure 12. Steady dimensionless thermal radius R_c^* as a function of N_{surf} for $N_{base} = 0$ and $N_\lambda = 0.5$. For $N_{surf} \gg 1$, $R_c^* \approx 1$, whereas R_c^* scales as $N_{surf}^{-1/2}$ for $N_{surf} \ll 1$. This behavior is valid for any N_λ .

lava flows, the duration of the transient stage scales as the diffusive time τ , which varies as one-half power of the effusion rate and the viscosity (equation (9)).

[35] Table 4 presents the predictions of our formalism for three kinds of hot geological gravity currents: (1) subaerial basaltic lava flows on Earth and on the Jovian satellite Io,

(2) a viscous silicic lava dome, and (3) a mud volcano. The orders of magnitude of the transient time t_c , of the steady radiated heat flux $\overline{\phi_{rad}}$ and of the radius of the thermal anomaly R_c are calculated using the estimated values of the dimensionless numbers and our first-order model. On small planetary bodies such as Io, the absence of an atmosphere suppresses convective cooling and makes the cooling less efficient, thus yielding a higher transient cooling time t_c .

5.2. Comparison With Natural Lava Flows and Domes

[36] Lava domes often display an axisymmetric geometry, and have been modeled as gravity currents [Huppert *et al.*, 1982]. The approach of Harris *et al.* [2007b] has previously been applied to retrieve the extrusion rate of a lava dome [Harris *et al.*, 2003; van Manen *et al.*, 2010]. However, our model predicts that the thermal steady state, implicit in Harris' thermal proxy [Harris *et al.*, 1997a], will only be reached after years of continuous supply rate, due to the high viscosity of silicic magma (Table 4). As the growth of volcanic domes is discontinuous with activity periods from a few days to several years [Barmin *et al.*, 2002; Wadge *et al.*, 2010], cooling of the emplaced material between two injections is likely to prevent the establishment of a thermal steady state. For example, the radiance of a dome with the parameters of Table 4 and supplied continuously at $5 \text{ m}^3 \text{ s}^{-1}$ is after 1 year only 20% of the steady value, leading to a similar underestimation of the extrusion rate. This underestimation is reinforced by the limited exposure of fresh lava at the dome surface through a cool rock carapace [Kaneko *et al.*, 2002; Wright *et al.*, 2002; Vaughan and Hook, 2006].

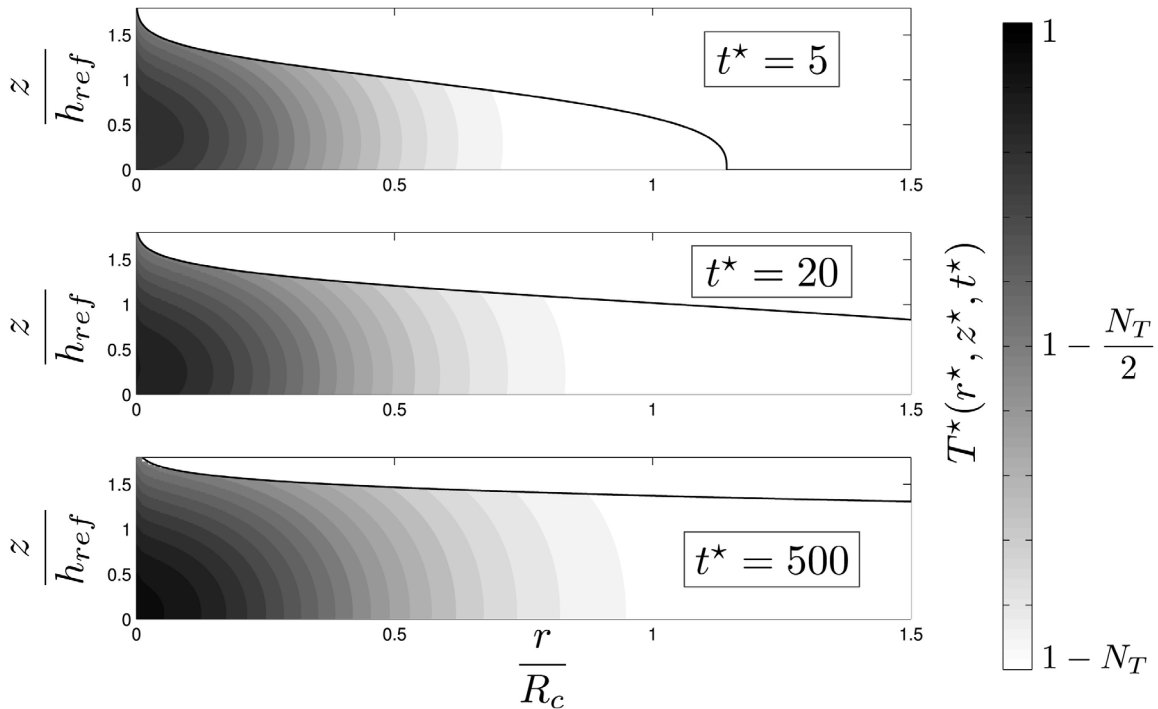


Figure 13. Temperature structure at different times in a current with $N_T = 0.5$, $N_\lambda = 0.5$, $N_{surf} = 1$, and $N_{base} = 1$. The initial positive vertical temperature gradient at the base of current evolves at long times toward an adiabatic profile as in Figure 6.

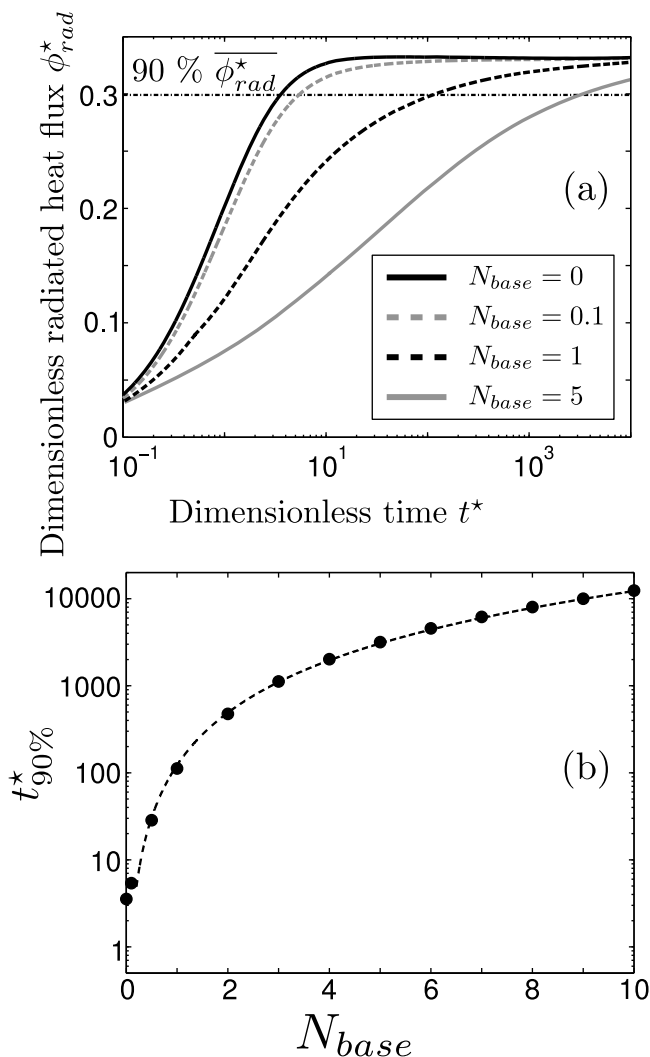


Figure 14. Influence of basal conduction on the cooling of a viscous gravity current. (a) Dimensionless radiated heat flux ϕ_{rad}^* as a function of time for different values of N_{base} . The other dimensionless numbers are $N_T = 0.5$, $N_\lambda = 0.5$, and $N_{surf} = 1$. (b) Transient time $t_{90\%}^*$ as a function of N_{base} . The dashed line is proportional to N_{base}^2 .

[37] The vertical and global thermal structure of a compound lava flow field is more complex than the one achieved in our model (Figures 2 and 10) [Hon *et al.*, 1994; Harris *et al.*, 2007a]. Furthermore, the effusion rate is likely to vary during an effusive eruption [Wadge, 1981; Coltelli *et al.*, 2007], and a steady state is expected only if the time scale of the variations is larger than the transient diffusive time. Hence the increase of radiance observed at the onset of some basaltic eruptions [Harris *et al.*, 1997b; Wooster *et al.*, 1997; Hirn *et al.*, 2009] may correspond to the transient thermal stage with a constant effusion rate rather than to an increase in the effusion rate.

[38] We are interested in the comparison of our theoretical predictions with measurements of the global heat flux radiated by lava flows. Table 5 presents this comparison for three different eruptions, where both a ground-based effusion rate and a radiated heat flux were available. The formalism of

Harris *et al.* [2007b] and ours agree well with the field observations, despite their simplifications, and we may wonder why such crude models do work. An explanation is the robustness of the energy balance between the heat injected into the system and the heat loss at the surface at long times. Axisymmetric gravity currents with complex rheology were also predicted to eventually reach a thermal steady state [Bercovici and Lin, 1996; Balmforth and Craster, 2000; Balmforth *et al.*, 2004], suggesting a secondary role of rheology for this thermal balance. Furthermore, following arguments by Walker [1973], we expect that a flow on an inclined plane will also attain this thermal equilibrium: for a given flow rate, the current flowing on a slope will get thinner and cover a larger area, but will also cool more rapidly.

[39] On the other hand, we expect that the surface thermal signal will not reflect the flow dynamics in the case of lava tubes, because the low crust temperatures do not reflect a potentially high flow rate of hot lava underneath [Realmuto *et al.*, 1992]. The simple thermal proxies yield correct orders of magnitude because they are restricted to eruptions without major lava tube systems (lava tubes formed only in some parts of the flow in phase V of the 1991–1993 Etna eruption reported by Calvari and Pinkerton [1998]). Finally, the exact predicted values for the effusion rate are affected by the chosen thermal and physical parameters [Harris *et al.*, 2007b] (Table 4). These empirical factors may compensate a departure from the modeled value of the steady radiated heat flux due to topography and rheology, and the fact that old cooling parts of the lava flow field may be integrated in the total radiant budget.

6. Conclusion

[40] In this paper, we have developed a thermal model for the cooling of an axisymmetric isoviscous gravity current whose spreading can be described by the theory of Huppert [1982]. Our model includes surface cooling by radiation and convection, and basal cooling by conduction to a substrate. The model predictions, validated by laboratory experiments, show that this cooling isoviscous gravity current fed at a constant rate first undergoes a transient thermal stage, and later reaches a stationary surface thermal state.

[41] Although simplified, our model provides some orders of magnitude for the steady radiated heat flux of currents fed at a constant rate that can be compared to field or remote sensed thermal surveys of natural lava flows. The model predicts that the steady radiated heat flux, reached after a transient time that scales as the diffusive time, is primarily set by the effusion rate. The order of magnitude of the effusion rate retrieved from radiated power in the case of three natural lava flows is in agreement both with ground-based measurements and with the estimations of the thermal proxy derived by Harris *et al.* [2007b]. Moreover, our model is able to scale the duration of the transient stage, which is a first-order estimate for the time scale over which the “time-averaged discharge rate” of Wright *et al.* [2001] and Harris *et al.* [2007b] is averaged indeed.

[42] We do not yet model the effect of slope nor of temperature-dependent viscosity, but the presented, consistent model of an isoviscous axisymmetrical gravity current will provide a sound scaling for the better understanding

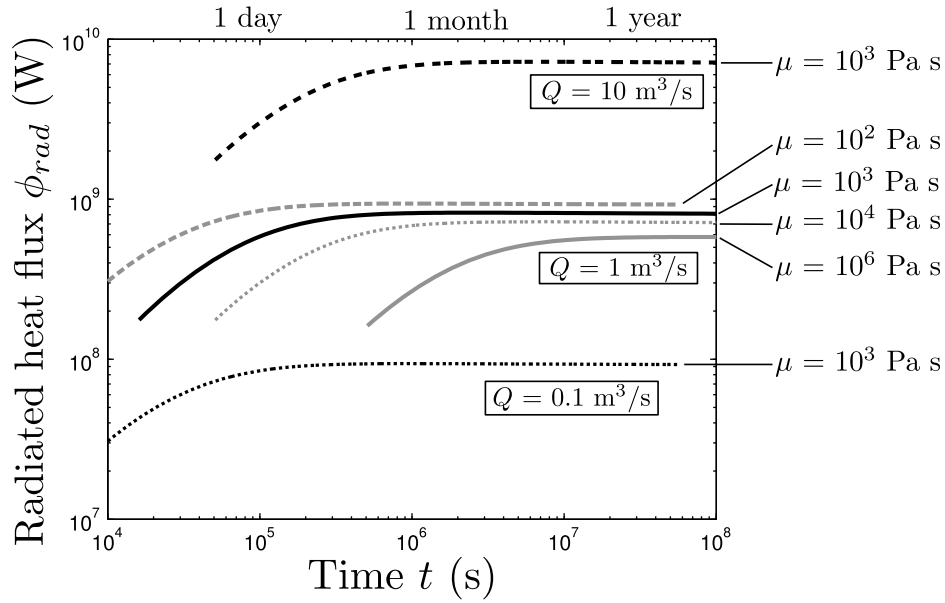


Figure 15. Theoretical evolution of the heat flux radiated by an isoviscous lava flow spreading on an adiabatic substrate for a viscosity $\mu = 10^3$ Pa s (black lines) and effusion rates Q of 0.1 (dotted line), 1 (solid line), or $10 \text{ m}^3 \text{ s}^{-1}$ (dashed line). The gray lines correspond to $Q = 1 \text{ m}^3 \text{ s}^{-1}$ with viscosities μ of 10^2 (dashed line), 10^4 (dotted line), or 10^6 Pa s (solid line). The other physical parameters are the same as in Table 4.

Table 4. Parameters, Dimensionless Numbers, and Scales of the Steady State for Natural Gravity Currents^a

| | Lava Flow | | | Lava Dome | Mudflow |
|--|-------------------|--------------------|--------------------|-----------------------------------|--------------------|
| | On Earth (Small) | On Earth (Large) | On Io ^b | | |
| g ($\text{m}^2 \text{ s}^{-1}$) | 9.8 | 9.8 | 1.8 | 9.8 | 9.8 |
| ρ^c (kg m^{-3}) | 2300 | 2300 | 2300 | 2300 | 1300 |
| μ (Pa s) | 10^3 | 10^3 | 10^3 | 10^9 | 20 |
| Q ($\text{m}^3 \text{ s}^{-1}$) | 1 | 100 | 1000 | 0.1–5 ^d | 0.1 |
| T_0 ($^\circ\text{C}$) | 1100 | 1100 | 1600 | 700 | 50 |
| T_{air} ($^\circ\text{C}$) | 20 | 20 | −140 | 20 | 20 |
| κ ($\text{m}^2 \text{ s}^{-1}$) | 10^{-6} | 10^{-6} | 10^{-6} | 10^{-6} | 7×10^{-7} |
| k ($\text{W K}^{-1} \text{ m}^{-1}$) | 3 | 3 | 3 | 3 | 1 |
| λ^e ($\text{W K}^{-1} \text{ m}^{-2}$) | 10 | 10 | 0 | 10 | 10 |
| h_{ref} (m) | 0.5 | 1.5 | 4 | 9–23 | 0.1 |
| τ | 2 days | 21 days | 5 months | 2–13 years | 5 h |
| N_T | 0.8 | 0.8 | 0.93 | 0.7 | 0.1 |
| N_λ | 0.07 | 0.07 | 0 | 0.16 | 0.84 |
| N_{surf} | 25 | 78 | 575 | 174–462 | 1.4 |
| $T_{top}(r=0)$ ($^\circ\text{C}$) | 250 | 130 | 100 | 50–33 | 31 |
| R_c | 500 m | 7 km | 60 km | 530 m–6 km | 120 m |
| S_c^f (km^2) | 0.8 | 164 | 12 000 | 0.9–112 | 0.04 |
| $\overline{\phi}_{rad}$ (W) | 0.8×10^8 | 6×10^{10} | 2×10^{12} | 6×10^7 – 3×10^9 | 10^6 |
| t_c^g | 3.5 days | 23 days | 15 months | 2–13 years | 11 h |

^aFor all cases, the emissivity ϵ is taken equal to 0.97 and the specific heat C_p is $1000 \text{ J kg}^{-1} \text{ K}^{-1}$.

^bAfter Davies [1996] and Davies *et al.* [2001]. Williams *et al.* [2001b, 2001a] computed much lower viscosity around 1 Pa s, for which the flow would be turbulent and our model could not apply.

^cThe low-density value for lava accounts for vesicularity [Harris *et al.*, 2007b].

^dRange of dome growth rate after Barmin *et al.* [2002] and Wadge *et al.* [2010].

^eIn the case of free convection for lava flows, evaluated by Neri [1998].

^fThe surface of the thermal anomaly at steady state is $S_c = \pi R_c^2$.

^gThe transient time is given for an adiabatic conditions at the base of the current ($N_{base} = 0$).

Table 5. Comparison of Effusion Rates Measured on the Field and Assessed by the Thermal Proxies

| Eruption ^a | Date | Thermal Survey | Radiant Flux | Effusion Rates (m ³ s ⁻¹) | | |
|-----------------------|---------------------------|-----------------|-------------------|--|---|-------------------------|
| | | | | Field | Method of <i>Harris et al.</i> [2007b] | This Study ^b |
| Etna | Jun 1992 to Mar 1993 | ATSR, AVHRR | 2–3 GW | 1–15 ^c | 5–8 | 3–4 |
| Etna | 29 Jul 2001 | MIVIS | 4 GW ^d | 6–10 ^e | 4–9 | 6 |
| Reunion Island | 29 Jun 2003 to 3 Jul 2003 | infrared camera | 90 MW | 0.1 ± 0.05 ^f | 0.25 | 0.1 |

^aEtna 1991–1993: *Calvari et al.* [1994], *Tanguy et al.* [1996], *Wooster et al.* [1997], and *Harris et al.* [1997a]; Etna 2001: *Behncke and Neri* [2003], *Coltelli et al.* [2007], and *Lombardo et al.* [2009]; Reunion Island 2003: *Coppola et al.* [2005, 2010].

^bParameters of Table 4, with either $T_0 = 1050^\circ\text{C}$ (Etna) or $T_0 = 1200^\circ\text{C}$ (Reunion Island). The measured radiated heat flux is assumed to be the steady one.

^cMean output rate during the whole eruption around $5 \text{ m}^3 \text{ s}^{-1}$ but higher in the earlier phases.

^dFlow F4 that started on 18 July.

^eHigh effusion rates around $15\text{--}30 \text{ m}^3 \text{ s}^{-1}$ several days before.

^fEffusion rate of $0.8 \text{ m}^3 \text{ s}^{-1}$ on 25 June.

of more complex models. Monitoring the evolution of the surface thermal signal of a lava tube system would also be crucial to better assess the limitation of thermal proxies. Another important issue is the “buffering” of the thermal signal following rapid variations of the effusion rates, and the coupled evolution of radiant signal and flow area. Finally we hope that this study will motivate the development of high-frequency acquisition techniques of the heat flux radiated by lava flows to provide new data constraints on the models.

Appendix A: Experimental Geometry of the Current

[43] For each of the 15 experiments we performed (Table 1), the radial extent of the current $R_N(t)$ is retrieved from the optical images corrected for distortion. For each experiment, we calculate the best fit coefficient a_{exp} of equation (8), reproducing quite well the experimental data (Figure A1).

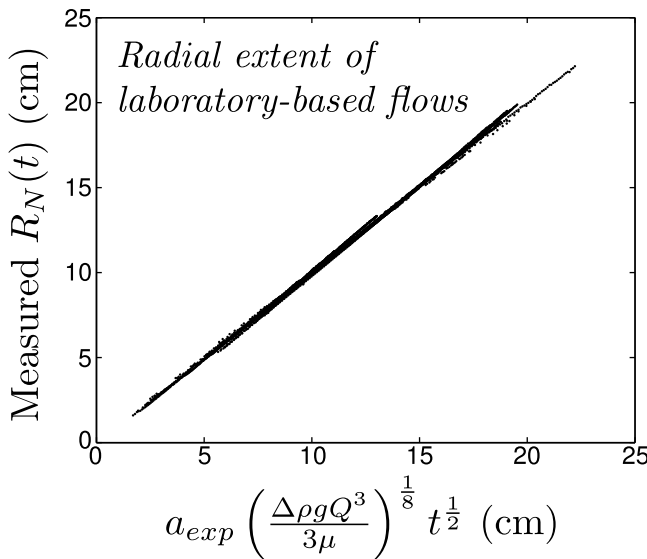


Figure A1. Measured versus theoretical radius $R_N(t)$. The black dots represent over 3200 measurements made during 15 experiments. The best fit values of a_{exp} are given in Table A1 for each experiment.

[44] The best fit values of a_{exp} presented in Table A1 are higher for the experiments where the oil flowed over Teflon ($\overline{a_{exp}} \approx 0.763 \pm 0.02$) than the ones with the plastic film ($\overline{a_{exp}} \approx 0.674 \pm 0.01$), possibly due to a higher surface tension in the former case. These two distinct values bracket the theoretical coefficient 0.715 proposed by *Huppert* [1982].

[45] The current thickness is directly measured on photographs taken by a lateral camera at different times during experiment C7. The experimental shape function $\psi(r^*) = \frac{h(r,t)}{h_{ref}}$ is compared in Figure A2 with its predicted numerical solution and an approximate theoretical solution

$$\psi(r^*) = \left(\frac{3}{2}\right)^{\frac{1}{3}} (1 - r^*)^{\frac{1}{3}} \left[1 + \frac{1}{12}(1 - r^*) + O((1 - r^*)^2)\right], \quad (\text{A1})$$

which corrects the approximation given in equation 2.27 of *Huppert* [1982]. A bulge with a constant width is present above the feeding pipe. The bulge shrinks in the dimensionless frame r^* due to the time evolution of $R_N(t)$ and becomes negligible for $t^* > 10$. It prevents however the use of a time-independent Gaussian fit, as suggested by *Stasiuk*

Table A1. Best Fit Experimental Spreading Coefficients^a

| Experiment | a_{exp} |
|------------|-----------|
| M4 | 0.680 |
| M5 | 0.682 |
| M10 | 0.698 |
| M13 | 0.669 |
| M23 | 0.683 |
| M17 | 0.651 |
| M18 | 0.669 |
| M19 | 0.658 |
| M20 | 0.678 |
| C1 | 0.746 |
| C7 | 0.779 |
| F2 | 0.735 |
| F5 | 0.745 |
| F6 | 0.753 |
| C14 | 0.782 |

^aIn the “M” experiments the polystyrene substrate is covered with a thin plastic film and the oil is injected from above, whereas in the “F” and “C” experiments the substrate is covered with a Teflon film and the injection is made from below.

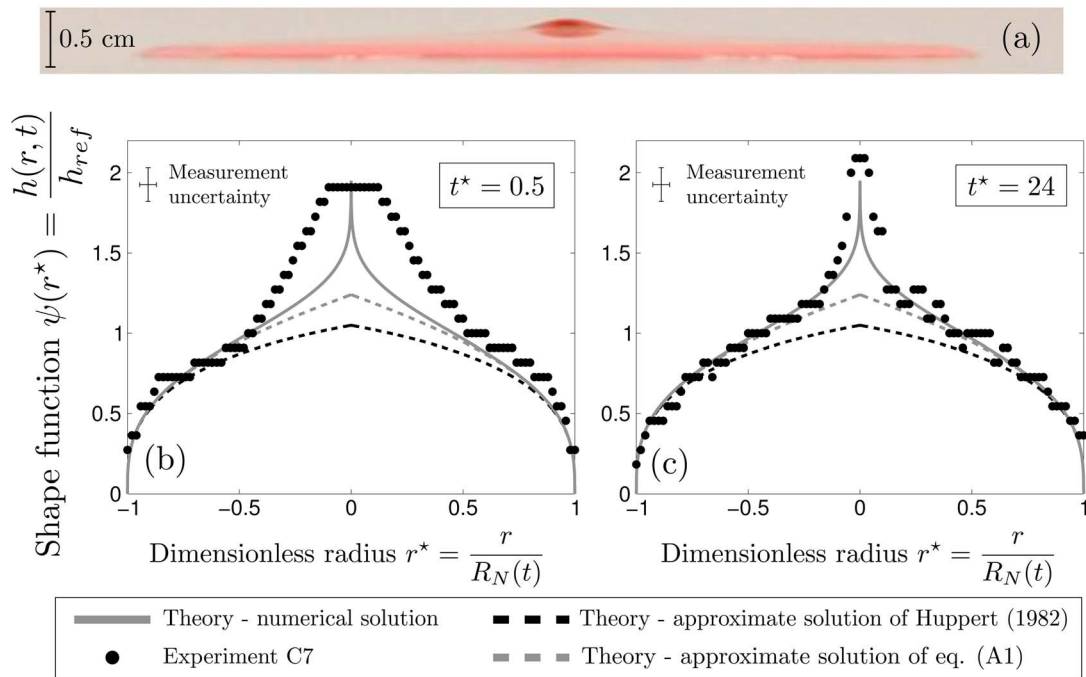


Figure A2. (a) Visible lateral photograph taken during experiment C7 at $t^* = 6$. Normalized height data at (b) $t^* = 0.5$ and (c) $t^* = 24$. The extent of the flow is $R_N = 1.5$ cm (Figure A2a) and $R_N = 9.7$ cm (Figure A2b). The flow contours are identified on a pixel-by-pixel basis. The corrected approximate solution of ψ at order 2 (equation (A1)) is closer to the numerical solution than the one given by Huppert [1982]. The central bulge above the feeding pipe is steady in the r frame and therefore shrinks in the r^* frame as a function of time.

and Jaupart [1997], to account for the experimental data at small times.

[46] An independent comparison between the numerical height solution and the experimental data is shown in Figure A3 based on a noninvasive colorimetric technique (Appendix B) used on 165 photographs taken during experiment M13. For each photograph, the mean shape is calculated on about ten different profiles across the oil pancake. We do not have access to the part of the current hidden by the pipe (Figure A4). The numerical solution of the shape function ψ appears again in full agreement with the experimental data.

Appendix B: Colorimetric Technique for Height Measurements

[47] The height of the current is retrieved from a visible image with a noninvasive colorimetric technique, derived from the Beer-Lambert's law [Taisne, 2008]:

$$I = I_0 e^{-hc}, \quad (\text{B1})$$

where I is the intensity of the green component of the oil on the picture, I_0 is the intensity of the green component of the plate with no oil on a reference picture, h is the thickness of the oil and c is related to the concentration of dye in the oil. Equation (B1) is valid for light transmitted through the oil, when the light source is placed underneath the thin polystyrene plate (experiments M10, M13, and M23, Figure A4a) and assumes null reflection at the fluid-air boundary. The

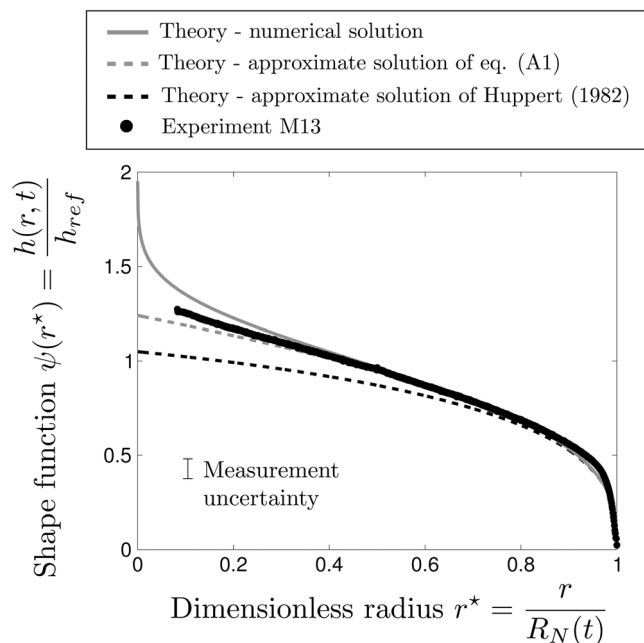


Figure A3. Experimental (M13) and theoretical shape functions ψ . The experimental shape function represents the mean over 165 visible images during experiment M13 between $t = 75$ s and $t = 875$ s, with 10 profiles across the oil pancake (Appendix B) for each photograph.

constant c is evaluated knowing the total oil volume V at the time the picture was taken:

$$Q \times t = V = \iint_{\text{oil pancake}} h dx dy = \frac{1}{c} A_{\text{pixel}} \sum_{\text{pixels in the oil pancake}} \ln\left(\frac{I_0}{I}\right), \quad (\text{B2})$$

with A_{pixel} the surface of a pixel on the picture. A continuous height profile can be retrieved using this technique (Figure A4b).

[48] This technique also provides a neat visualization of the advance of the gravity current with a detailed shape at the flow front (Figure B1). The contact angle between oil, air and the plastic film at the front remains quite constant throughout the experiment.

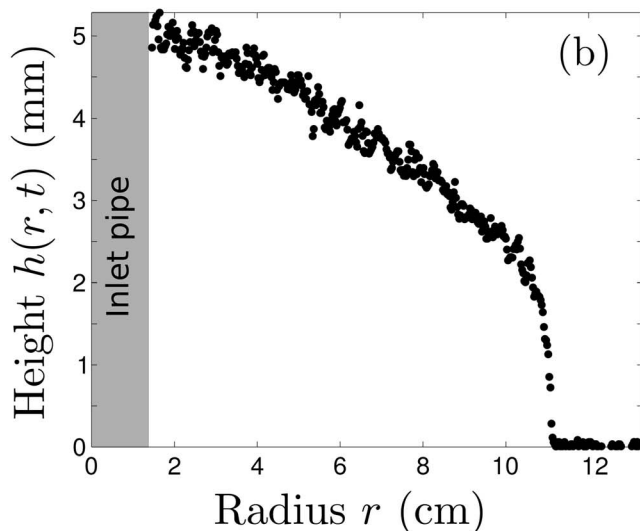
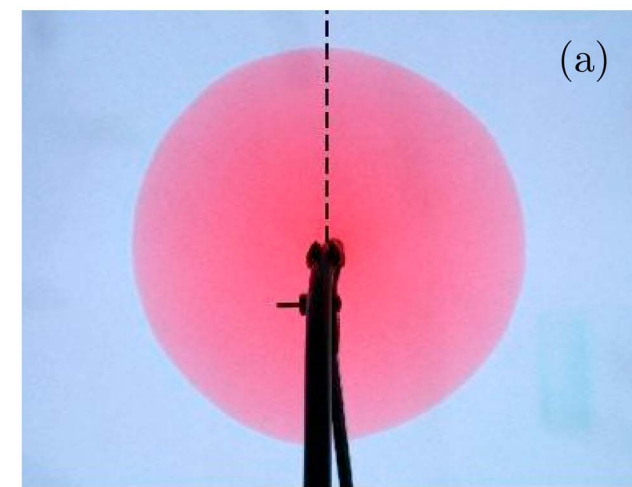


Figure A4. (a) Photograph of experiment M13, with the light transmitted through the thin polystyrene plate and an injection from above. (b) Height calculated using the colorimetric technique as a function of distance from the source on the profile (dashed line) shown in Figure A4a. The uncertainty on height measurements is around 0.2 mm. For each photograph, the height is retrieved from several profiles across the oil pancake.

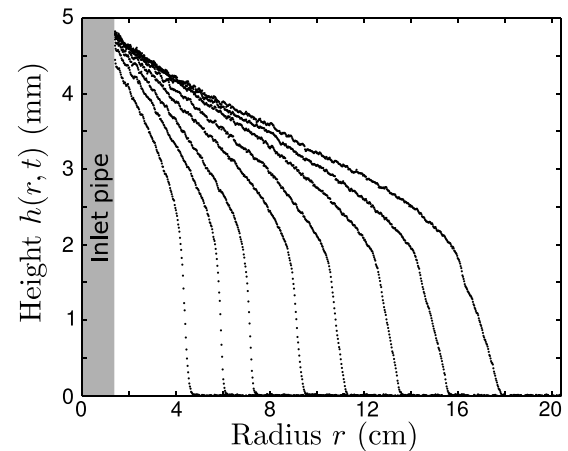


Figure B1. Advance and shape of the flow front with time for experiment M10. The different flow shapes are calculated by averaging several profiles across the pancakes at $t = 69, 119, 169, 269, 369, 519, 669,$ and 844 s.

[49] **Acknowledgments.** We acknowledge Yves Gamblin and Antonio Vieira for their help with the experimental device, as well as Benoît Taisne for the colorimetric technique. We greatly thank Patrick Richon and Damien Gaudin for the lending of their infrared cameras. This paper has benefited from careful reviews of the Associate Editor Michael P. Ryan and of two anonymous reviewers, as well as from useful comments by David Bercovici, Ross Griffiths, and Stephen Blake on an earlier version of this manuscript.

References

- Ancey, C., and S. Cochard (2009), The dam-break problem for Herschel-Bulkley viscoplastic fluids down steep flumes, *J. Non Newtonian Fluid Mech.*, *158*(1–3), 18–35.
- Balmforth, N. J., and R. V. Craster (2000), Dynamics of cooling domes of viscoplastic fluid, *J. Fluid Mech.*, *422*, 225–248.
- Balmforth, N. J., R. V. Craster, and R. Sassi (2004), Dynamics of cooling viscoplastic domes, *J. Fluid Mech.*, *499*, 149–182.
- Balmforth, N. J., R. V. Craster, A. C. Rust, and R. Sassi (2006), Viscoplastic flow over an inclined surface, *J. Non Newtonian Fluid Mech.*, *139*(1–2), 103–127.
- Barmin, A., O. Melnik, and R. Sparks (2002), Periodic behavior in lava dome eruptions, *Earth Planet. Sci. Lett.*, *199*(1–2), 173–184.
- Behncke, B., and M. Neri (2003), The July–August 2001 eruption of Mt. Etna (Sicily), *Bull. Volcanol.*, *65*(7), 461–476.
- Bercovici, D. (1994), A theoretical model of cooling viscous gravity currents with temperature-dependent viscosity, *Geophys. Res. Lett.*, *21*, 1177–1180, doi:10.1029/94GL01124.
- Bercovici, D., and J. Lin (1996), A gravity current model of cooling mantle plume heads with temperature-dependent buoyancy and viscosity, *J. Geophys. Res.*, *101*(B2), 3291–3309, doi:10.1029/95JB03538.
- Blake, S., and B. C. Bruno (2000), Modelling the emplacement of compound lava flows, *Earth Planet. Sci. Lett.*, *184*(1), 181–197.
- Calvari, S., and H. Pinkerton (1998), Formation of lava tubes and extensive flow field during the 1991–1993 eruption of Mount Etna, *J. Geophys. Res.*, *103*(B11), 27,291–27,301, doi:10.1029/97JB03388.
- Calvari, S., M. Coltelli, M. Neri, M. Pompilio, and V. Scribano (1994), The 1991–1993 Etna eruption: Chronology and lava flow-field evolution, *Acta Vulcanol.*, *4*, 1–14.
- Carslaw, H. S., and J. C. Jaeger (1959), *Conduction of Heat in Solids*, 510 pp., Oxford Univ. Press, Oxford, U. K.
- Coltelli, M., C. Proietti, S. Branca, M. Marsella, D. Andronico, and L. Lodato (2007), Analysis of the 2001 lava flow eruption of Mt. Etna from three-dimensional mapping, *J. Geophys. Res.*, *112*, F02029, doi:10.1029/2006JF000598.
- Coppola, D., T. Staudacher, and C. Cigolini (2005), The May–July 2003 eruption at Piton de la Fournaise (La Reunion): Volume, effusion rates, and emplacement mechanisms inferred from thermal imaging and global positioning system (GPS) survey, in *Kinematics and Dynamics of Lava Flows*, edited by M. Manga and G. Ventura, *Spec. Pap. Geol. Soc. Am.*, *396*, 103–124.

- Coppola, D., M. James, T. Staudacher, and C. Cigolini (2010), A comparison of field- and satellite-derived thermal flux at Piton de la Fournaise: Implications for the calculation of lava discharge rate, *Bull. Volcanol.*, 72(3), 341–356.
- Davies, A. G. (1996), Io's volcanism: Thermo-physical models of silicate lava compared with observations of thermal emission, *Icarus*, 124(1), 45–61.
- Davies, A. G., et al. (2001), Thermal signature, eruption style, and eruption evolution at Pele and Pillan on Io, *J. Geophys. Res.*, 106, 33,079–33,103, doi:10.1029/2000JE001357.
- Dragoni, M., and A. Tallarico (2009), Assumptions in the evaluation of lava effusion rates from heat radiation, *Geophys. Res. Lett.*, 36, L08302, doi:10.1029/2009GL037411.
- Fink, J. H., and R. W. Griffiths (1990), Radial spreading of viscous-gravity currents with solidifying crust, *J. Fluid Mech.*, 221, 485–509.
- Griffiths, R. W., and J. H. Fink (1992), Solidification and morphology of submarine lavas: A dependence on extrusion rate, *J. Geophys. Res.*, 97(B13), 19,729–19,737, doi:10.1029/92JB01594.
- Griffiths, R. W., and J. H. Fink (1997), Solidifying Bingham extrusions: A model for the growth of silicic lava domes, *J. Fluid Mech.*, 347, 13–36.
- Griffiths, R. W., R. C. Kerr, and K. V. Cashman (2003), Patterns of solidification in channel flows with surface cooling, *J. Fluid Mech.*, 496, 33–62.
- Harris, A., and S. Baloga (2009), Lava discharge rates from satellite-measured heat flux, *Geophys. Res. Lett.*, 36, L19302, doi:10.1029/2009GL039717.
- Harris, A., S. Blake, D. Rothery, and N. Stevens (1997a), A chronology of the 1991 to 1993 Mount Etna eruption using advanced very high resolution radiometer data: Implications for real-time thermal volcano monitoring, *J. Geophys. Res.*, 102(B4), 7985–8003, doi:10.1029/96JB03388.
- Harris, A., A. Butterworth, R. Carlton, I. Downey, P. Miller, P. Navarro, and D. Rothery (1997b), Low-cost volcano surveillance from space: Case studies from Etna, Krafla, Cerro Negro, Fogo, Lascar and Erebus, *Bull. Volcanol.*, 59(1), 49–64.
- Harris, A., W. Rose, and L. Flynn (2003), Temporal trends in lava dome extrusion at Santiaguito 1922–2000, *Bull. Volcanol.*, 65(2), 77–89.
- Harris, A., J. Dehn, M. James, C. Hamilton, R. Herd, L. Lodato, and A. Steffke (2007a), Pahoehoe flow cooling, discharge, and coverage rates from thermal image chronometry, *Geophys. Res. Lett.*, 34, L19303, doi:10.1029/2007GL030791.
- Harris, A., J. Dehn, and S. Calvari (2007b), Lava effusion rate definition and measurement: A review, *Bull. Volcanol.*, 70(1), 1–22.
- Hirn, B., C. Di Bartola, and F. Ferrucci (2009), Combined use of SEVIRI and MODIS for detecting, measuring, and monitoring active lava flows at erupting volcanoes, *IEEE Trans. Geosci. Remote Sens.*, 47(8), 2923–2930.
- Hon, K., J. Kaahikaua, R. Denlinger, and K. Mackay (1994), Emplacement and inflation of pahoehoe sheet flows: Observations and measurements of active lava flows on Kilauea volcano, Hawaii, *Geol. Soc. Am. Bull.*, 106(3), 351–370.
- Huppert, H. E. (1982), The propagation of two-dimensional and axisymmetric viscous gravity currents over a rigid horizontal surface, *J. Fluid Mech.*, 121, 43–58.
- Huppert, H. E., J. B. Shepherd, H. Sigurdsson, and R. S. J. Sparks (1982), On lava dome growth, with application to the 1979 lava extrusion of the Soufriere de St. Vincent, *J. Volcanol. Geotherm. Res.*, 14(3–4), 199–222.
- Kaminski, E., S. Tait, F. Ferrucci, M. Martet, B. Hirn, and P. Husson (2011), Estimation of ash injection in the atmosphere by basaltic volcanic plumes: The case of the Eyjafjallajökull 2010 eruption, *J. Geophys. Res.*, 116, B00C02, doi:10.1029/2011JB008297.
- Kaneko, T., M. Wooster, and S. Nakada (2002), Exogenous and endogenous growth of the Unzen lava dome examined by satellite infrared image analysis, *J. Volcanol. Geotherm. Res.*, 116(1–2), 151–160.
- Lombardo, V., A. Harris, S. Calvari, and M. F. Buongiorno (2009), Spatial variations in lava flow field thermal structure and effusion rate derived from very high spatial resolution hyperspectral (MIVIS) data, *J. Geophys. Res.*, 114, B02208, doi:10.1029/2008JB005648.
- Lyman, A. W., E. Koenig, and J. H. Fink (2004), Predicting yield strengths and effusion rates of lava domes from morphology and underlying topography, *J. Volcanol. Geotherm. Res.*, 129(1–3), 125–138.
- Michaut, C., and D. Bercovici (2009), A model for the spreading and compaction of two-phase viscous gravity currents, *J. Fluid Mech.*, 630(1), 299–329.
- Neri, A. (1998), A local heat transfer analysis of lava cooling in the atmosphere: Application to thermal diffusion-dominated lava flows, *J. Volcanol. Geotherm. Res.*, 81(3–4), 215–243.
- Pieri, D. C., and S. M. Baloga (1986), Eruption rate, area, and length relationships for some Hawaiian lava flows, *J. Volcanol. Geotherm. Res.*, 30(1–2), 29–45.
- Realmutu, V., K. Hon, A. Kahle, E. Abbott, and D. Pieri (1992), Multi-spectral thermal infrared mapping of the 1 October 1988 Kupaianaha flow field, Kilauea volcano, Hawaii, *Bull. Volcanol.*, 55(1), 33–44.
- Sakimoto, S., and M. Zuber (1995), The spreading of variable-viscosity axisymmetric radial gravity currents: Applications to the emplacement of Venusian ‘pancake’ domes, *J. Fluid Mech.*, 301(1), 65–77.
- Sakimoto, S. E. H., and T. K. P. Gregg (2001), Channeled flow: Analytic solutions, laboratory experiments, and applications to lava flows, *J. Geophys. Res.*, 106, 8629–8644, doi:10.1029/2000JB900384.
- Stasiuk, M. V., and C. Jaupart (1997), Lava flow shapes and dimensions as reflections of magma system conditions, *J. Volcanol. Geotherm. Res.*, 78(1–2), 31–50.
- Stasiuk, M. V., C. Jaupart, and R. S. J. Sparks (1993), Influence of cooling on lava-flow dynamics, *Geology*, 21(4), 335–338.
- Taisne, B. (2008), Vicissitudes de l’ascension des magmas à travers la croûte terrestre, PhD thesis, Inst. de Phys. du Globe de Paris, Paris.
- Tallarico, A., and M. Dragoni (2000), A three-dimensional Bingham model for channeled lava flows, *J. Geophys. Res.*, 105(B11), 25,969–25,980, doi:10.1029/2000JB900201.
- Tanguy, J., G. Kieffer, and G. Patanč (1996), Dynamics, lava volume and effusion rate during the 1991–1993 eruption of Mount Etna, *J. Volcanol. Geotherm. Res.*, 71(2–4), 259–265.
- van Manen, S., J. Dehn, and S. Blake (2010), Satellite thermal observations of the Bezymianny lava dome 1993–2008: Precursory activity, large explosions, and dome growth, *J. Geophys. Res.*, 115, B08205, doi:10.1029/2009JB006966.
- Vaughan, R., and S. Hook (2006), Using satellite data to characterize the temporal thermal behavior of an active volcano: Mount St. Helens, WA, *Geophys. Res. Lett.*, 33, L20303, doi:10.1029/2006GL027957.
- Wadge, G. (1981), The variation of magma discharge during basaltic eruptions, *J. Volcanol. Geotherm. Res.*, 11(2–4), 139–168.
- Wadge, G., R. Herd, G. Ryan, E. Calder, and J. Komorowski (2010), Lava production at Soufrière Hills Volcano, Montserrat: 1995–2009, *Geophys. Res. Lett.*, 37, L00E03, doi:10.1029/2009GL041466.
- Walker, G. (1973), Lengths of lava flows, *Philos. Trans. R. Soc. London A*, 274, 107–116.
- Williams, D., R. Greeley, R. Lopes, and A. Davies (2001a), Evaluation of sulfur flow emplacement on Io from Galileo data and numerical modeling, *J. Geophys. Res.*, 106, 33,161–33,174, doi:10.1029/2000JE001340.
- Williams, D. A., A. G. Davies, L. P. Keszthelyi, and R. Greeley (2001b), The summer 1997 eruption at Pillan Patera on Io: Implications for ultrabasic lava flow emplacement, *J. Geophys. Res.*, 106, 33,105–33,119, doi:10.1029/2000JE001339.
- Wooster, M., R. Wright, S. Blake, and D. Rothery (1997), Cooling mechanisms and an approximate thermal budget for the 1991–1993 Mount Etna lava flow, *Geophys. Res. Lett.*, 24, 3277–3280, doi:10.1029/97GL03166.
- Wright, R., S. Blake, A. J. L. Harris, and D. A. Rothery (2001), A simple explanation for the space-based calculation of lava eruption rates, *Earth Planet. Sci. Lett.*, 192(2), 223–233.
- Wright, R., S. De La Cruz-Reyna, A. Harris, L. Flynn, and J. Gomez-Palacios (2002), Infrared satellite monitoring at Popocatepetl: Explosions, exhalations, and cycles of dome growth, *J. Geophys. Res.*, 107(8), 2153, doi:10.1029/2000JB000125.
- Wright, R., L. Flynn, H. Garbeil, A. Harris, and E. Pilger (2004), MODVOLC: Near-real-time thermal monitoring of global volcanism, *J. Volcanol. Geotherm. Res.*, 135(1–2), 29–49.

F. Garel, E. Kaminski, A. Limare, and S. Tait, Équipe de Dynamique des Fluides Géologiques, Institut de Physique du Globe de Paris, Sorbonne Paris Cité, Université Paris Diderot, UMR CNRS 7154, 1 rue Jussieu, F-75005 Paris, France. (garel@ipgp.fr)